# PU.1 Eviction at Lymphocyte-Specific Chromatin Domains Mediates Glucocorticoid Response in Acute Lymphoblastic Leukemia

Duohui Jing（✉ jdh12262@rjh.com.cn ）
  Shanghai Institute of Hematology, State Key Laboratory of Medical Genomics, National Research Center for Translational Medicine at Shanghai, Ruijin Hospital Affiliated to Shanghai Jiao Tong Universi   https://orcid.org/0000-0002-1491-8002

**Dominik Beck**
  Centre for Health Technologies and the School of Biomedical Engineering, University of Technology

**Honghui Cao**
  Shanghai Institute of Hematology, State Key Laboratory of Medical Genomics, National Research Center for Translational Medicine at Shanghai, Ruijin Hospital Affiliated to Shanghai Jiao Tong Universi

**Feng Tian**
  School of Medicine, Institute of Biomedical Informatics, Hebei University of Engineering, Handan, Hebei Province, 056038, China

**Yizhou Huang**
  Children's Cancer Institute, Lowy Cancer Research Centre, School of Clinical Medicine, UNSW Medicine & Health, UNSW Centre for Childhood Cancer Research, UNSW Sydney

**Han Zhao**
  Shanghai Institute of Hematology, State Key Laboratory of Medical Genomics, National Research Center for Translational Medicine at Shanghai, Ruijin Hospital   Shanghai Jiao Tong University Sch

**Xiaolu Tai**
  Department of Plastic and Reconstructive Surgery, Shanghai Ninth People's Hospital, Shanghai Jiao Tong University School of Medicine, Shanghai, China

**WENQIAN XU**
  Shanghai Institute of Hematology, State Key Laboratory of Medical Genomics, National Research Center for Translational Medicine at Shanghai, Ruijin Hospital Affiliated to Shanghai Jiao Tong Universi

**Hansen Kosasih**
  Children's Cancer Institute, Lowy Cancer Research Centre, School of Clinical Medicine, UNSW Medicine & Health, UNSW Centre for Childhood Cancer Research, UNSW Sydney

**David Kealy**
  Centre for Blood Research, University of York

**Katherine Bridge**
  Centre for Blood Research, University of York

**Weiye Zhao**
  York Biomedical Research Institute, University of York

**Andrew Holding**
  York Biomedical Research Institute, University of York

**Adam Dowle**
  Metabolomics & Proteomics Laboratory, Bioscience Technology Facility, Department of Biology, University of York

**Samuel Taylor**
  Department of Cell Biology, Albert Einstein College of Medicine

**Gaoxian Song**
  Shanghai Institute of Hematology, State Key Laboratory of Medical Genomics, National Research Center for Translational Medicine at Shanghai, Ruijin Hospital Affiliated to Shanghai Jiao Tong Universi

**Diego Fajardo**
  Centre for Health Technologies and the School of Biomedical Engineering, University of Technology

**Yashna Walia**
  Children's Cancer Institute, Lowy Cancer Research Centre, School of Clinical Medicine, UNSW Medicine & Health, UNSW Centre for Childhood Cancer Research, UNSW Sydney

**Meng Wang**

Department of Plastic and Reconstructive Surgery, Shanghai Ninth People's Hospital, Shanghai Jiao Tong University School of Medicine, Shanghai, China   https://orcid.org/0000-0003-0221-0653

Chao Zhang

Shanghai JiaoTong University   https://orcid.org/0000-0001-6418-8370

Jin Wang

Shanghai Institute of Hematology, State Key Laboratory of Medical Genomics, National Research Center for Translational Medicine at Shanghai, Ruijin Hospital Affiliated to Shanghai Jiao Tong Universi

Jian-Qing Mi

State Key Laboratory of Medical Genomics, Shanghai Institute of Hematology, Rui Jin Hospital Affiliated to Shanghai Jiao Tong University (SJTU) School of Medicine, 197 Rui Jin Road II, Shanghai

Richard Lock

Children's Cancer Institute

Charles de Bock

Children's Cancer Institute, University of New South Wales   https://orcid.org/0000-0001-5182-8535

---

Article

Keywords:

Additional Declarations: There is **NO** Competing Interest.

---

# Abstract

The epigenetic landscape plays a critical role in the onset and evolution of various malignancies, but its therapeutic utility remains underutilized. Glucocorticoids are an essential part of many multi-agent treatment regimens for lymphoid malignancies. However, the emergence of glucocorticoid resistance is a significant barrier to cure, which is in part due to epigenetic alterations, including aberrant chromatin accessibility and hypermethylation at lymphocyte-specific glucocorticoid-response elements (GREs). To gain a deeper understanding of regulatory mechanisms leading to these epigenetic alterations, we conducted a multi-omics study, including chromosome conformation capture sequencing (HiC), to examine changes in the 3D genome structure following the *in vivo* treatment of acute lymphoblastic leukemia (ALL) patient-derived xenografts (PDXs) with glucocorticoid. We found that glucocorticoid treatment led to distinct patterns of topologically associated domains (TADs) in glucocorticoid sensitive compared to resistant PDXs. Furthermore, we show that these TADs were primed by the development-related pioneer transcription factor PU.1, which extensively interacts with the glucocorticoid receptor (GR) exclusively in glucocorticoid-sensitive ALL PDXs. An integrative analysis of rapid immunoprecipitation mass spectrometry of endogenous protein (RIME) and ChIP-seq revealed that PU.1 binding was associated with lymphocyte-specific activation of GREs and GRE-interacting super-enhancers. The PU.1-associated TADs modulated epigenetic marks, and particularlythe eviction of PU.1 promoted GR binding and the expression of signature genes, including *BIM*, *ZBTB16* and *RASA1*, mediating glucocorticoid-induced apoptosis in ALL. These findings were phenocopied using a PU.1 inhibitor DB2313 to restore glucocorticoid sensitivity in ALL. Taken together, this study identified a new epigenetic pathway integrating PU.1 priming and PU.1-GR interaction which ultimately leads to PU.1 eviction in ALL. This pathway provides the first link between the activity of a lineage-specific transcription factor and epigenetic modulators mediating the response to glucocorticoids and thus offers a new avenue to translate fundamental epigenetic research into the clinic.

# Main

Acute lymphoblastic leukemia (ALL) is the most common cancer among children. Glucocorticoids, such as prednisone and dexamethasone, are critical components of most multi-agent chemotherapy regimens used to treat lymphoid malignancies[1–4]. However, the emergence of glucocorticoid resistance remains a significant barrier to cure[3–5], glucocorticoid-based therapies rarely successfully treat myeloid malignancies[6], and the molecular basis for these observations remains elusive[7,8].

Glucocorticoids function via interactions with the glucocorticoid receptor (GR) in the cytoplasm[9], after which the GR translocates to the nucleus to act as a transcription factor (TF) by binding to accessible glucocorticoid-response elements (GREs)[10–12]. The accessibility of GREs can be characterized by histone H3 modifications (e.g., H3K4Me3 and H3K27Ac) at cis-regulatory elements[13,14]. We have previously identified a series of cis-regulatory conditions (i.e., low accessibility and hypermethylation at GREs) associated with glucocorticoid resistance in ALL[15–18]. However, upstream mechanisms responsible for regulating the epigenetic landscape at GR binding sites remain elusive.

Whole exome and transcriptome sequencing has identified many genetic and epigenetic mutations in relapsed/refractory ALL[15,19–27]. Although various mechanisms for glucocorticoid resistance have been proposed, they do not converge into a single common cause for all patients. For instance, loss of *BTG1* or *PTEN* can cause glucocorticoid resistance by inhibiting GR expression or translocation to the nucleus[28,29], but primary ALL cells rarely show blocked GR function[23]. Similarly, even though some ALLs exhibit mutations in epigenetic regulators, such as *KMT2D*, *CREBBP* and *HDAC7*, no specific mutations account for abnormal chromatin accessibility across all patients. Nonetheless, the significance of *BIM* as a key gene in glucocorticoid-induced apoptosis in ALL is well recognized. Mutations in various genes that deregulate different signaling pathways[30–33], have been associated with the dysregulation of *BIM* and glucocorticoid resistance. We have demonstrated that epigenetic abnormalities at lymphocyte-specific genes, including an enhancer of *BIM*[15], and mutation in methyltransferase gene *NSD2*[18], occur in ALLs with normal and mutant karyotypes, and contribute to the development of glucocorticoid resistance. Importantly, while the high diversity of genetic mutations might prohibit the discovery of a unified genetic cause for drug resistance, epigenetic variation, including chromatin accessibility and methylation are much more common characteristics of relapsed/refractory ALL.

Lineage-specific pioneer TFs, such as PU.1, EBF1 and TCF3, can initiate nucleosome remodelling during lymphocyte development, regulate the transcription of lineage-specific genes[34,35], and recruit TET2 and DNMT3b to modulate DNA methylation of target genes, which in turn regulates gene expression during hematopoietic differentiation[36]. Chromatin conformation provides a structural framework for TF binding and thus gene regulation[37,38]. From 0.8 million open chromatin domains identified by DNase I-hypersensitive site (DHS) sequencing (derived from ENCODE), we have previously defined over 11,000 lymphocyte-specific open chromatin domains (LSOs)[15]. By analyzing glucocorticoid-induced epigenetic alterations in ALL patient-derived xenografts (PDXs) *in vivo*, we identified around 2,000 LSOs with GR binding (GR-LSOs), including 42 GR-activated and 61 GR-repressed LSOs with abnormal hypermethylation in glucocorticoid-resistant ALL.

Although the precise mechanism by which lineage-specific pioneer factors contribute to the epigenetic aberrations seen at GR-LSOs in ALL are unknown, here, we hypothesize that the activity of these factors during tumor evolution primes regulatory domains which in turn leads to abnormal chromatin remodeling and the development of glucocorticoid resistance in ALL. In this study, we aimed to explore common upstream events that contribute to the aberrant chromatin accessibility patterns that we have previously described in ALL, and to identify new targets, and strategies for reversing glucocorticoid resistance.

# Results

## Distinct Regions of Higher Order Chromatin are Associated with Dexamethasone Response in ALL

To explore the relationship between chromatin conformation and glucocorticoid response, we conducted chromosome conformation capture sequencing (HiC) in two pediatric ALL PDXs following dexamethasone (DEX) treatment *in vivo*. Both PDXs have normal cytogenetics and comparative basal gene expression profiles but ALL-54S is sensitive and ALL-50R is resistant to DEX *in vivo* and *in vitro*[15,25].

We first integrated the HiC measures with our database of epigenetic profiles from a previous study of the same PDXs[15]. The genome was divided into 60,000 bins, each with a size of 50kb, and we compared their principal components (PCA, representing contact intensities) across 0.8 million DHS domains in ALL-54S and ALL-50R. Analysis of these data showed that regions with an increasing signal of open chromatin (Low to High DHS) also had an increasing number of HiC interactions (PCA Value) in both PDXs, validating the principles of nuclear organization from other publications[39] (**Supplementary Table S1** and Fig. 1A, **first panel**). Representative genomic regions of DHS-Low, -Mid, and -High bins are shown in **Supplementary Figure S1A**. Focusing on LSOs and LSCs (i.e. DHS domains open and closed in lymphocytes, respectively), HiC contact intensities were higher in LSOs (Fig. 1A) with a trend for increasing contact intensities for genome regions (50 kb bins) that contained higher frequencies of LSOs (**Figure S1B**). LSOs that were also bound by the GR[15], showed somewhat higher contact intensities compared to those without GR binding (non-GR-LSOs) (Fig. 1A). Finally, limiting our analyses to the subset of the 42 activated and 61 repressed GR-LSOs (i.e. associated with changes in key gene expressions[15]), we found that the ALL-54S PDX had higher basal contact intensity that increased upon *in vivo* DEX treatment for the 42 activated GR-LSOs but remained the same for ALL-50R, while no difference was observed for the 61 repressed GR-LSOs (Fig. 1A, **fourth panel**).

Next, we determined DEX-induced chromatin conformation changes on a genome-wide scale (**Supplementary Table S2**). Most contact intensities remained unchanged (i.e., stable) but we found a ~ 2-fold increase in dynamic changes (i.e. bins with increasing or decreasing contact intensities) in ALL-54S compared to ALL-50R (Fig. 1B). Therefore, we set out to identify bins that showed significantly different contact intensities between sensitive and resistant cells post-treatment with DEX (i.e., ALL-54S and ALL-50R). In total, 4645 bins were significantly different, including 135 dynamic bins containing GR-LSOs and their associated genes including the previously identified *BIM* (*BCL2L11*). (**Supplementary Table S3**, Fig. 1C**). Combining the dynamic changes and overlaying with the 42 GR-activated and 61 GR-repressed LSOs in ALL-50R and ALL-54S (Fig. 1D), we further identified a number of regions containing genes of interest, including *ZBTB16*, *BCL2L11* (*BIM*), *SUPT4H1*, and others linked to aberrant chromatin accessibility and glucocorticoid resistance[15,19−27]. These data suggest that the ability to dynamically change higher-order chromatin interactions is key to GR sensitivity, warranting further interrogation on regulatory factors of chromatin conformation.

### PU.1 is a Transcriptional Regulator of Higher Order Chromatin Regions Associated with DEX Response in ALL

To better understand the cis-regulatory mechanism of these chromatin conformation dynamics and their associated response to DEX we performed an enrichment analysis using i-cisTarget to identify potential upstream regulators[40,41]. Our *in silico* analysis focussed on GR-LSOs enriched for H3K27Ac (Enhancer mark) in ALL-54S but not ALL-50R post-DEX treatment (**Supplementary Table S4**). The DNA binding motifs for 77 TFs were identified with the highest enrichment scores found for steroid receptor family members with similar motifs including the GR (as expected), the androgen receptor (AR) and the mineralocorticoid receptor (MR), as well as for motifs of key TFs involved in lymphocyte development, such as PU.1, EBF1, and TCF3 (Fig. 2A, **Supplementary Table S5)**. However, while many motifs shared common binding domains, PU.1 (SPI1) had the highest enrichment score among ETS family proteins which was comparable to GR (i.e., median NES of 3.01 vs 3.25), while EBF1 had the highest score among non-ETS family proteins (i.e., median NES of 0.88), and the structural protein CTCF exhibited no enrichment (median NES of -0.19; Fig. 2B).

To complement this *in silico* analysis and directly identify GR co-factors that mediate tissue-specific effects of glucocorticoids, we performed rapid immunoprecipitation mass spectrometry (RIME) analysis[42] of GR-binding proteins in ALL-54S and ALL-50R post-DEX treatment (Fig. 2C). Our data showed that the PU.1 protein was significantly enriched in the DEX-treated GR pulldown over the GR pulldown from the same PDX under control conditions for ALL-54S but not for ALL-50R. There was no significant enrichment for ELF1, EBF1, or CTCF proteins in

either condition. Together, the *in-silico* prediction and RIME experimentation provide compelling evidence for PU.1, rather than any other ETS family members or structural proteins, as a coregulator of GR.

This finding led to a global analysis of PU.1 binding in ALL-54S and ALL-50R by ChIP-seq and using the structural protein CTCF as control. Comparing binding profiles in dynamic bins pre- and post-treatment with DEX, we found that CTCF binding remained unchanged, while PU.1 binding was globally decreased in ALL-54S but not ALL-50R (Fig. 2D). These data suggest that the interaction between GR and PU.1 might lead to the eviction of PU.1 at dynamic bins (i.e. HiC) after the treatment with DEX and this further warrants a study of PU.1 and GR co-binding on these regulatory domains.

### PU.1 Eviction Mediates DEX Response Via Recruitment of the GR in DEX Sensitive but not Resistant ALLs

Next, binding profiles of GR, PU.1 and CTCF at key clusters of glucocorticoid-response genomic regions, i.e. LSCs, LSOs, non-GR-LSOs, and GR-LSOs, were analyzed (Fig. 3A). We found that the GR and PU.1 were bound more frequently to LSOs than LSCs (green curves vs. orange curves) while CTCF binding was generally low and did not exhibit any group preference. Furthermore, while PU.1 was enriched at both GR-LSOs and non-GR-LSOs, its enrichment was much stronger at GR-LSOs, providing further evidence for the cooperation of PU.1 and the GR at LSOs. Moreover, we have previously shown that there was no difference in chromatin accessibility (ATAC-seq) or CTCF binding (ChIP-seq) at either GR-LSOs or non-GR-LSOs in ALL-54S and ALL-50R[15]. However, when we interrogated our new datasets, we found that PU.1 binding at GR-LSOs and non-GR-LSOs, showed a marked difference between ALL-54S and ALL-50R (Fig. 3B). In response to DEX treatment, the binding of PU.1 increased in ALL-50R but decreased in ALL-54S for GR-LSOs and non-GR-LSOs.

To further explore these patterns, we also interrogated PU.1 binding at each individual GR-LSO upon DEX treatment, and used CTCF and another lineage-specific TF EBF1 as controls. We found that sites exclusively bound by PU.1 decreased by 7% and those bound by both PU.1 & EBF1 decreased by 8% in ALL-54S (Fig. 3C; **Supplementary Table S6**). These losses were accompanied by an 8% and 7% increase in sites lacking TF binding or sites bound exclusively by EBF1, respectively. In line with these data, among the 1773 GR-LSOs, 1009 did not show any changes in the binding patterns of PU.1, EBF1, and CTCF in ALL-54S (depicted by black bars in Fig. 3D). However, we identified three patterns of GR-LSOs in ALL-54S, consisting of 127, 97, and 39 sites, which exclusively exhibited loss of PU.1 binding while maintaining an unchanged pattern of EBF1 and CTCF binding (depicted by blue bars in Fig. 3D). As a control, the top two patterns of GR-LSOs with EBF1 changes demonstrated 48 exclusive losses and 41 exclusive gains of EBF1 in ALL-54S (depicted by green bars in Fig. 3D). In contrast, the PU.1 eviction upon DEX treatment was not observed in ALL-50R (**Supplementary Figure S2A and B**), and PU.1 binding in ALL-50R revealed a similar pattern to EBF1 (positive z-score) in a bootstrapping analysis compared to a distinct action of the PU.1 in ALL-54S (negative z-score; **Figure S2C**).

Taken together, these data suggest that PU.1 primes chromatin in treatment-naive cells, and that PU.1 eviction is linked to GR binding post-treatment with DEX, in sensitive but not resistant leukemia cells.

### PU.1 Priming and Eviction Lead to Epigenetic Changes at GREs and the Formation of a Densely Connected Gene Regulatory Network with the GR

Next, we integrated the above data with regions of open chromatin (ATAC-Seq) in gene regulatory elements defined by the presence of the histone modifications H3K4Me3 (promoter region), H3K4Me1 (enhancer region), H3K27Ac (active region) and H3K27Me3 (repressed region). Using these histone marks, the genome was partitioned into regulatory regions including promoters, enhancers and dual promotor-enhancer regions. These were then further divided into silent (S), active (A), repressed (R) and bivalent (Bi) regions (Fig. 4A). Reconciling these regions with the ChIP-seq data, CTCF and PU.1 were more frequently bound at repressed regions when compared to the GR across all conditions, while PU.1 but not CTCF was more frequently bound to enhancers than promoters. However, we also found differences between conditions, for example, PU.1 showed a different binding frequency at active enhancers in ALL-54S compared to ALL-50R (Fig. 4A). Similarly, at GR-LSOs, the binding patterns of GR and PU.1 were constrained to the distribution of the GR-LSOs (**Supplementary Figure S3A**). Taken together, while these data show that high GR enrichment was critical for the activation of promoters and enhancers, a low enrichment of PU.1 was associated with enhancer activation in ALL-54S.

Furthermore, we associated the gene promoters within GR-LSOs and their target genes using HiC (**Supplementary Table S7**) and then integrated these data with gene expression measured by RNA-Seq. Unsupervised hierarchical clustering analysis of differentially expressed genes identified four clusters which variably correlated with the identity of gene regulatory elements (**left panel in** Fig. 4B). For example, in ALL-54S, we found that H3K27Ac in clusters 1 and 2 (red box, indicating active enhancers and promoters) was increased and in line with up-regulated gene expression but remained unchanged in clusters 3 and 4 despite the downregulation of target genes - suggesting that additional factors might impact the down-regulated genes (**right and lower panel in** Fig. 4B). Interestingly, we found that the genomic regions of cluster 2 had a significant decrease in PU.1 binding in ALL-54S but not ALL-50R (**Supplementary Figure S3B**). In ALL-50R, however, H3K27Me3 levels were elevated at promoters of selected target genes (green boxes), including *BIM* and *ZBTB16*, and this was in line with their

stable gene expression pre/post DEX treatment (**left panel in** Fig. 4B). These data suggest that genes differentially regulated in ALL-50R and ALL-54S, including *BIM* and *ZBTB16*, are associated with H3K27Ac and H3K27Me3 at genomic regions bound by PU.1.

To further elucidate potential signaling pathways regulated by the GR-interacting protein networks, we performed an ingenuity pathway analysis of genes and proteins identified from RNA-seq and RIME experiments (Fig. 4C). RIME analyses demonstrated that the "gene expression pathway" was the most enriched upon DEX treatment, validating the critical role of GR-interacting proteins in triggering gene transcription. Both RNA-seq and RIME analyses demonstrated that up- or down-regulated genes or GR protein-protein interactions were significantly enriched in "cellular development, proliferation, death & survival pathways" (involving both pro- and anti-apoptotic genes), and "cell cycle pathways". This suggests that the GR and its interacting proteins cooperate to induce proliferation arrest and cell death of ALL cells following DEX treatment *in vivo*. Particularly, as the most significant one on the list, enrichment of the "cellular development pathway" is consistent with interaction of the GR with the lineage-specific transcriptional factor PU.1 in response to glucocorticoid treatment.

Next, we used Cytoscape[43] to construct a regulatory network model centred around GR-LSOs by integrating data from i-cisTargets motif analyses of GR and PU.1 compared to some control lineage-specific TFs such as EBF1 and TCF3 (Fig. 4D). This analysis revealed a core set of genes that are co-regulated by GR and PU.1, compared to rare connections between the GR and two other TFs (EBF1 and TCF3). *ZBTB16*, a regulator of lymphoid development[44], had multiple connections with both the GR and PU.1. *ZBTB16* was also ranked highly in two independent analyses of DEX-induced HiC contact intensities (Figs. 1C **and D)** and an integrative transcriptome and epigenome analysis (RNA-seq, H3K27Ac/me3 and H3K4me1/me3 ChIP-Seq; Fig. 4B), which suggests that *ZBTB16* may play a role in the GR - PU.1 pathway and might thus be a mediator of DEX response in ALL.

### Multi-omics Annotation of DEX-Induced De Novo TADs Confirms the Eviction of PU.1 as a Recurrent Epigenetic Pattern in DEX Sensitive but not Resistant ALLs

We next compared changes in topological associated domain (TAD) formation pre- and post-treatment with DEX in the sensitive and resistant PDXs, and found that the formation of DEX-induced *de novo* TADs is common at genomic regions surrounding GR-LSOs. First, our analysis identified the formation of a *de novo* TAD spanning a 300kb region around the *BIM* LSO in ALL-54S but not ALL-50R (Fig. 5A **top**). This TAD had two contact-enriched sub-regions, including a breakpoint at the *BIM* enhancer[15], and ΔHiC analysis confirmed an increase in contact frequency in ALL-54S but a decrease in frequency in ALL-50R post-treatment with DEX (Fig. 5A **bottom**). In ALL-50R, the decrease was in-line with a lack of conclusive protein binding at the TAD borders (i.e., CTCF marked only one of the two TAD borders) pre- and post-treatment. In ALL-54S, however, we found an overall increase in contact frequencies which was particularly high in regions adjacent to its borders post-treatment (Fig. 5B, **top**). CTCF marked both TAD borders and PU.1 was bound adjacent to both TAD borders pre- but not post-treatment. The LSO was bound by CTCF pre- and post-treatment, by PU.1 pre- but not post-treatment, and by the GR and H3K27Ac post- but not pre-treatment (Fig. 5B, **bottom**). Notably, *BIM* expression was also upregulated post-treatment, while *ACOXL* expression, a gene located upstream to the TAD, remained unchanged (Fig. 5F).

Similarly, we identified the formation of *de novo* TADs surrounding GR-LSOs at *ZBTB16* and *RASA1* loci (Figs. 5C **and Supplementary Figure S4A)**, which followed the same epigenetic blueprint pre- and post-treatment with DEX (Figs. 5D and S4B). The TAD at the *ZBTB16* locus was again divided into three sub-sections by the LSO and its two TAD borders (Fig. 5C). Interestingly, we found a relatively larger increase in contact intensities in the sub-section downstream of the LSO insulated by the two TAD borders. In ALL-54S, but not ALL-50R, the treatment led to a particularly high increase in H3K27Ac, and this region was thus identified as a 32kb sized super-enhancer (SE) by ROSE[45] (*ZBTB16* SE, Fig. 5D). In ALL-54S and ALL-50R, both TAD borders were insulated by CTCF, further shifting our focus to the interaction between the LSO, the *ZBTB16* SE, and other gene regulatory elements. In ALL-54S, but not ALL-50R, and in line with our previous observations, the binding of PU.1 was partly lost, and the binding of the GR and H3K27Ac partly gained, post-treatment at both the LSO and *ZBTB16* SE (Fig. 5D), and particularly, interactions between *ZBTB16* SE and genes located within the TAD were critically enhanced post-treatment (Fig. 5E). This was consistent with activation of *ZBTB16* and other genes within the TAD, including *ZW10*, *USP28* and *H3TR3A* post-treatment (Fig. 5F). Of note, genes such as *TMPRSS5* located at the upstream border of the TAD and *H3TR3B* showing no interaction with the *ZBTB16* SE, revealed no response to DEX treatment.

The LSO and the *ZBTB16* promoter interacted more frequently with the *ZBTB16* SE in ALL-54S than ALL-50R and we found an additional increase in interactions post-treatment in ALL-54S (**Supplementary Figure S4D and E**). Additionally, the LSO also interacted more frequently with the SE, compared to the promoter, suggesting that *ZBTB16* is regulated by the LSO via the SE in ALL. Furthermore, a genome-wide HiC study revealed upregulated SE activities at IN HiC dynamic bins in ALL-54S post-DEX treatment, compared to that in ALL-50R, indicating SE may play an important role in mediating chromatin conformation dynamics in response to glucocorticoid (**Figure S4F**).

To assess these observations across a larger panel of sensitive vs. resistance ALL samples upon dexamethasone treatment *in vivo*, ATAC-seq studies were performed to determine chromatin accessibility at the *ZBTB16* locus (Fig. 5G). While the *ZBTB16* SE seems commonly open in

sensitive and resistant ALL, the *ZBTB16* LSO is only accessible in glucocorticoid-sensitive PDXs but not resistant PDXs. These data indicate a more cell-type-specific role of the LSO rather than the SE in mediating glucocorticoid activities.

The multi-omics annotation of two TADs, at the *BIM* and *ZBTB16* loci, illustrate how TFs drive the cooperation of gene regulatory elements and super-enhancers to remodel chromatin, and identified a recurrent pattern of selective PU.1 eviction followed by recruitment of the GR and H3K27Ac in ALL-54S but not ALL-50R. This suggests PU.1 eviction as an upstream regulatory mechanism underlying DEX response in ALL.

### PU.1 Knockdown and Combination Treatment with the PU.1 Inhibitor DB2313 in ALL In Vitro and In Vivo

To validate the function of the LSO and SE at the *ZBTB16* locus, we identified six H3K27Ac-enriched regions within the *ZBTB16* SE (**Figure S5A**) and performed luciferase reporter assays (Fig. 6A). Interestingly, while the full-length *ZBTB16* LSO did not significantly enhance luminescence we found that the insertion of SE peaks #2 and #6 significantly increased luciferase expression upon DEX treatment in Nalm6 cells (**Figure S5B**). Next, we performed luciferase reporter assays with the PU.1 inhibitor DB2313. When compared to the treatment with DEX alone, combination treatment with DB2313 significantly increased the luminescence intensities from *BIM, RASA1* and the *ZBTB16* LSO-insert in Nalm6 cells (Fig. 6A).

We have recently demonstrated that the sensitivity of PU.1 to displacement by DB compounds is reliant upon an enrichment of A/T nucleotides surrounding the core PU.1 ETS motif (Fig. 6B, **left panel**, Taylor et al., under review[46]). We find that GR-LSOs displayed a higher log-odds score for the "sensitive PU.1 motif" than non-GR-LSOs (Fig. 6B, **right panel**), suggesting that PU.1 would more likely be displaced by DB compounds from GR-LSOs than non-GR-LSOs and predicts for potential synergy between DB2313 and glucocorticoids. This hypothesis was supported by two additional observations; firstly, a time-course analysis showed an increased expression for *BIM*, *RASA1* and *ZBTB16* after the combination treatment with DB2313 compared to DEX alone (Fig. 6C). Secondly, a combination treatment with DB2313 and DEX also showed a synergistic cytotoxic effect in Nalm6 cells (SynergyFinder score: 11.95; Fig. 6D **and Figure S6A**). These data suggest that inhibition of PU.1 enhanced the sensitivity of Nalm6 cells to the treatment with DEX.

To further test these findings, we developed an inducible CRISPR knockout system and performed *BIM* and *PU.1* knockout (KO) *in vivo* in ALL-54S. The dox-induced *BIM* KO led to DEX resistance and shorter event-free survival (EFS) while the *PU.1* KO significantly delayed leukemic growth and led to an increase in EFS in ALL-54S (Fig. 6E **and F**). To better understand the impact of gene editing at both *BIM* and *PU.1* target sites, we analyzed the insertions and deletions (INDELs) generated by CRISPR in the *BIM* KO and *PU.1* KO clones. INDELs in *BIM* clones displayed varying lengths in all frames while those in *PU.1* exclusively generated in-frame mutations with lengths being multiples of 3bp particularly for DEX treated mice (Fig. 6G **and H**). Protein structures of two representative *PU.1* mutants with 3 or 6 bp insertions were predicted using Aphafold2[47] (**Figure S6B**). The insertions are located 140 amino acids upstream of the DNA binding domain of the PU.1 protein and do not alter its core structure. This suggested that frame-shift mutations were lethal and the extended EFS post DEX treatment was due to loss of all frame-shift mutated *PU.1* KO clones and therefore evicted from GR binding sites whereas clones that retain PU.1 will be selected for during DEX treatment due to lack of eviction and conferring glucocorticoid resistance.

## Discussion

Epigenomic landscapes play a crucial role in the evolution of leukemia but their therapeutic utility has yet to be fully realized. Previous studies have defined the genomic and epigenomic landscapes that mediate glucocorticoid resistance in ALL[15,18] and this study identified the developmental pioneer TF PU.1 as a critical upstream regulator. Furthermore, glucocorticoids have been in clinical use for decades, and their tissue- and cell-specific activity is a recurring clinical observation[7,48]. To this end, this study revealed the molecular basis of glucocorticoid response, and this could further be exploited to guide the clinical application of glucocorticoids and form a foundation for developing novel strategies to reverse resistance in ALL.

We have published a series of studies on epigenetic inhibition of the pro-apoptotic *BIM* gene associated with glucocorticoid resistance in ALL[15,23,25,49,50]. Dysregulation of a novel intronic GR-bound enhancer at the *BIM* locus that triggers *BIM* transcription and apoptosis of ALL upon glucocorticoid treatment was attributed to glucocorticoid resistance in ALL for the first time[25]. It was further demonstrated that the *BIM* enhancer was lymphocyte-specific and can be activated in normal and malignant lymphoid cells. Furthermore, glucocorticoid resistance driven by different mutations harboured a similar mechanism: aberrant chromatin accessibility[17,18].

While cancer stem cells have been identified as the initiators of chemo-resistance and relapse in various tumor types[51−53] including acute myeloid leukemia, lymphoid cells at various developmental stages have been implicated in key biological activities of ALL, such as oncogenesis, chemo-resistance, and relapse[54−59]. Thus, the critical role of developmental factors in ALL biology is becoming increasingly evident. In this study, we provide evidence through both bioinformatic and experimental work that PU.1, a well-studied lineage-specific pioneer protein, is highly interacting with the GR and associated with TAD dynamics in ALL PDXs upon treatment with DEX. Even though various

transcription levels and mutations were identified at gene loci coding for PU.1 and other TFs that are potentially associated with TAD alterations (RNA-seq and whole exome sequencing assays in **Supplementary Figure S7 and Table S8**), no specific gene dysregulation or mutation has been identified in PDXs used in this study with an annotation of inducing function loss of the TFs. This suggests that TF mutations may not be a cause for the abnormal chromatin accessibility in glucocorticoid resistant ALL.

Alterations in tumor-associated TADs are often oncogenic, and DNA structural variation, together with enhancer-hijacking play critical roles in the oncogenesis of various cancer types[60,61]. Several recent studies identified recurrent changes of TADs in leukemia subtypes and suggested their application as genomic signatures to stratify leukemias[61−63]. In this study, we identified a similar pattern, and reported TADs associated with distinct patterns of PU.1 binding in DEX-sensitive vs. resistant ALL, and PU.1 priming of lineage-specific cis-regulatory elements, rendering them as accessible before GR binding, in DEX-sensitive but not resistant ALLs. Our findings suggest that the PU.1 priming and eviction are critical events leading to the formation of DEX-induced *de novo* TADs in ALL, which cannot be achieved by either the structural protein CTCF that stabilizes TADs or other developmental TFs such as EBF1 or TCF3.

Furthermore, the ZBTB family comprises a diverse group of TFs, with several members considered to be critical regulators of lymphoid cell development[64]. For example, MIZ-1 (coded by *ZBTB17*) regulates B-cell differentiation at early progenitor stages[65], while *ZBTB16* (PLZF) directs differentiation of the NKT cell lineage[44] and its translocations have been reported critical in driving leukemogenesis, such as *ZBTB16-RARA* in acute promyelocytic leukemia (APL)[66] and *ZBTB16-ABL1* in T-ALL[67,68]. Our data suggest that *ZBTB16* was combinatorially regulated by GR and PU.1 at its LSO and SE, leading to the formation of a *de novo* TAD.

Overall, while epigenetic changes underlying DEX resistance may differ across different ALLs, this multi-omics analyses provides insights into a pathway of developmental factors modulating cancer genomes and sheds light on the unified upstream mechanism of developmental pioneer factor PU.1. These findings provide the first link between the lineage-specific transcription factors, response to glucocorticoids and the activity of epigenetic modulators and provide a new path to translate fundamental epigenetic research into the clinic.

# Methods

### ALL Xenograft Model and Primary Patient Samples

The process by which continuous xenografts from ALL biopsies have been established in immunodeficient NOD/SCID interleukin (IL)-2 receptor gamma chain null (NSG) mice has been previously described in detail[15,25]. ALL biopsies were obtained for xenografting with informed, written consent approved by the Human Research Ethics Committees of the South Eastern Sydney Illawarra Area Health Service and UNSW Sydney. All animal studies had previous approval from the Animal Care and Ethics Committee of UNSW Sydney. The fidelity of all PDXs in our laboratory is routinely validated by high-density SNP (single nucleotide polymorphism) arrays as previously described[21].

### *In Vivo* Treatments, Sample Preparation and Analysis

ALL xenograft cells were inoculated by tail-vein injection into NSG mice, and engraftment was monitored weekly as previously described[15,25]. Mice were randomized and treated with either dexamethasone (15 mg/kg) or vehicle control by intraperitoneal injection when the %huCD45$^+$ cells in the peripheral blood reached certain percentages as follows:

1. 1% for *in vivo* drug efficacy studies. In brief, when huCD45$^+$ cells reached 1% in the peripheral blood, the ALL-engrafted mice were treated with either dexamethasone or vehicle control on weekdays for 4 weeks. The percentage of huCD45$^+$ cells in murine peripheral blood was monitored weekly. The engraftment burden of ALL cells in different mouse organs after drug treatments was calculated based on the average number of cells harvested and normalized as a percent of average control for each experiment[27].
2. > 70% for *in vitro* molecular biology experiments. Briefly, mice were treated when > 70% %huCD45$^+$ cells in the peripheral blood, and euthanized 8 hours thereafter. Cell suspensions of spleens were prepared, and mononuclear cells enriched to >97% human cells by density gradient centrifugation. After harvesting, cells were immediately resuspended in fetal calf serum (FCS) containing 10% DMSO, frozen and stored at liquid nitrogen for further use.

### Assessment of Dexamethasone Sensitivity

*In vitro* dexamethasone sensitivity was assessed by mitochondrial activity using Alamar Blue assay as described previously[15,25]. The half maximal inhibitory concentration (IC$_{50}$) was calculated from the dose response curves. *In vivo* dexamethasone sensitivity was determined by the leukemia growth delay (LGD, treated-control). The sensitivities of ALL cells to dexamethasone *in vitro* and *in vivo* have been described in our previous publications[15,25]. The PDXs were stratified into glucocorticoid sensitive or resistant groups based on their *in vitro* IC50 and *in vivo* LGD.

## Rapid Immunoprecipitation Mass Spectrometry (RIME)

RIME was done with some minor modifications to the original protocol[69]. Briefly, 1x10$^8$ cells were collected from ALL-54S or ALL-50R upon acute treatment with DEX or vehicle control (8 hours), pelleted and initially cross-linked using 2mM disuccinimidyl glutarate (DSG) in PBS for 20 min with shaking at RT. After pelleting the cells, the cells were resuspended in 1% formaldehyde in PBS and incubated at RT with shaking for 10 min to double-cross-linked the samples[42]. Crosslinking was quenched by the addition of glycine to a final concentration of 0.125M and an incubation at RT for 5 min. The cells were washed with ice-cold PBS, then resuspended in PBS containing protease inhibitors (PI). The nuclear fraction was extracted by resuspending the pellet in 1mL LB1 (50mM HEPES-KOH pH7.5, 140mM NaCl, 1mM EDTA, 10% glycerol, 0.5% Igepal CA-630, 0.25% Tritox X-100) containing PI, followed by rotating the samples at 4°C for 10 min. After pelleting the cells, cells were resuspended in 1mL LB2 (10mM Tris-HCl pH8.0, 200mM NaCl, 1mM EDTA, 0.5mM EGTA) containing PI, mixed by rotation at 4°C for 5 min, then pelleted. The cells were then resuspended in 300µl LB3 (10mM Tris-HCl pH8.0, 100mM NaCl, 1mM EDTA, 0.5mM EGTA, 0.1% Na-Deoxycholate, 0.5% N-laurosylsarcosine) containing PI, and sonicated for 7 cycles (30 seconds on, 30 seconds off). To the sonicated samples, 10% Triton X-100 in LB3 was added to a final concentration of 1%, followed by centrifugation at 20,000xg for 10 mins at 4°C to remove the debris. The supernatant, which is the nuclear fraction, was then collected for immunoprecipitation. Protein A/G magnetic beads (Thermo Fisher Scientific) were firstly blocked with Pierce Protein-Free PBS blocking buffer (Thermo Fisher Scientific) and resuspended in LB3 containig 1% Triton X-100. The blocked beads were incubated with the supernatant containing the nuclear fraction for 1 hour rotating at RT to preclear the samples. The pre-cleared samples were incubated with 10µg anti-NR3C1 antibody (Atlas Antibodies) for overnight at 4°C with rotation. The samples/antibody mixtures were then incubated with blocked beads for 1 hour at RT with rotation. The beads were washed 10 times with LiCl RIPA buffer (50mM HEPES pH7.6, 1mM EDTA, 0.7% Na-Deoxycholate, 1% Igepal CA-630, 0.5M LiCl), followed by washing twice in 100mM ammonium hydrogen carbonate (AMBIC) solution. The beads were further washed three times with 25mM AMBIC solution, before tryptic on-bead digestion was performed by adding 10µl of sequencing grade trypsin (0.02µg/µl in 25mM AMBIC solution) and incubating overnight at 37°C. Additional 10µl of sequencing grade trypsin (0.02µg/µl in 25mM AMBIC solution) was added to the beads, and on-bead digestion was performed for another 1 hour at 37°C. Supernatant containing peptides was collected and combined with TFA to give a final concentration 0.1%. Peptides were loaded onto EvoTip Pure tips for desalting and as a disposable trap column for nanoUPLC using an EvoSep One system. A pre-set EvoSep 100 SPD gradient was used with an 8 cm EvoSep C$_{18}$ Performance column (150 mm x 1.5 mm). The nanoUPLC system was interfaced to a timsTOF HT mass spectrometer (Bruker) with a CaptiveSpray ionisation source (Source). Positive PASEF-DIA, ESI-MS and MS$^2$ spectra were acquired using Compass HyStar software (version 6.2, Thermo). Instrument source settings were: capillary voltage, 1,500 V; dry gas, 3 l/min; dry temperature; 180°C. Spectra were acquired between $m/z$ 100-1,700. Custom TIMS settings were applied as: 1/K0 0.-1.60 V.s/cm$^2$; Ramp time, 100 ms; Ramp rate 9.42 Hz. PASEF-DIA acquisition specified DIA-windows of 25 Th width between 400-1201 Th and a mobility range of 0.6-1.43 1/K0. The total cycle time was 1.8 s. Collision energy was interpolated between 20 eV at 0.6 V.s/cm$^2$ to 59 eV at 1.6 V.s/cm$^2$. Peak lists in .d format were imported into DIA-NN software (ver. 1.8)[70] for identification and relative quantification. An *in-silico* spectral library was created from the human subset of SwissProt appended with common proteomic contaminants. The two-pass method was used in DIA-NN, first searching against the *in-silico* library then iterating against the DIA data from these samples for a second search. The search was run at 1% FDR. DIA-NN results in peptide-centric .tsv format were filtered to peptide q-values <0.01, then pivoted on protein accessions before further filtering to require a minimum of 2 unique peptides per protein match and protein q-values <0.01. For statistical comparison between groups, missing values were imputed with minimum values and differential abundance was tested using limma through the FragPipe-Analyst (http://fragpipe-analyst.nesvilab.org/), run as a local installation in R-shiny. Three biological replicates were used for each group and the Hochberg and Benjamini correction was used for multiple test correction.

## HiC Library Preparation and Sequencing

HiC was performed using a modified version of a previously described protocol[71]. Briefly, 10 million cells were collected and cross-linked in 10 ml of PBS containing 1% formaldehyde for 10 minutes at room temperature. The reaction was stopped by 0.125M glycine solution. Cross-linked cell pellet was used to prepare nuclei, which were subjected to digestion with restriction enzyme MboI followed by end-filling to create biotin-labeled blunt ends. Blunt ends were ligated by T4 DNA ligase at room temperature for 4 hours with rotation. Nuclei were digested with proteinase K and 10% sodium dodecyl sulfate (SDS) at 55°C for 30 minutes. Following sodium acetate and pure ethanol precipitation, DNA was isolated and dissolved in Tris buffer. DNA was sonicated using Bioruptor sonicator (Diagenode SA, Belgium) to obtain fragments ranging in size from 150 bp to 300 bp, followed by double-sided size selection using AMPure XP beads at 0.55X and 0.3X volume for HiC. Biotinylated HiC material was then purified using Dynabeads MyOne Streptavidin T1 beads (Life technologies, 65602). While on beads, DNA ends were blunt ended and dA tailed, followed by ligation of the Illumina sequencing adapter with T4 DNA ligase. PCR reactions were performed on beads involving 8 cycles of amplification (95°C for 2 min, followed by 94°C for 80 s, 65°C for 30 s, 72°C for 30 s). DNA library was size selected using 1.5% agarose gel to obtain fragments ranging in size from 400bp to 700bp. Sequencing was performed on the Illumina HiSeq 2500 to obtain 150bp paired-end reads at sequencing depth of 100 million reads per sample.

## ChIP-seq

ChIP and ChIP-seq were carried out as previously described[15,25]. Briefly, frozen PDX cells that were harvested from mice after dexamethasone or vehicle control treatment *in vivo* were revived from cryostorage, and fixed with 1% formaldehyde for 10 min at room temperature. Nuclei were extracted from fixed cells by 10 min incubation in lysis buffer (0.2% NP40 in 10 mM Tris buffer, pH 8.0) followed by centrifugation at 1250 × g for 5 min at 4 °C. Chromatin was fragmented using a Bioruptor sonicator (Diagenode SA, Belgium) on high power at 4 °C with 30 s on/off for 10 min. Separate immunoprecipitates were produced using immunoglobulin raised against GR (Cell Signaling, Danvers, MA, USA), CTCF (Cell Signaling), H3 histone (Millipore, Billerica, MA, USA), histone marks (H3K4Me3, H3K4Me1, H3K27Ac and H3K27Me3, Cell Signaling)  and processed according to the manufacturer's instructions. DNA from protein-associated complexes and corresponding input samples were recovered using phenol/chloroform/isoamyl alcohol with phase lock gel tubes (5 Prime, Hilden, Germany). The ChIP DNA samples were dissolved in 20 µl water, library amplified, and sequenced using Hiseq2500 platform for 50bp single-end reads at 20 million reads per sample.

## RNA-seq

For gene expression studies, RNA was extracted immediately after cell harvesting using the RNeasy Mini Kit (QIAGEN, Valencia, CA, USA), and RNA samples with integrity number (RIN) > 8.0 were sent to Novogene (Beijing, China) for library preparation and sequencing using Hiseq4000 platform for 150bp paired-end reads at 40 million reads per sample.

## HiC Data Analysis

HiC data were first trimmed and then mapped against hg19 human reference genome using runHi-C pipeline based on the 4DN consortium. Specifically, Burrows-Wheeler Aligner (BWA) was used for the FASTQ file alignment and low-quality aligned reads and PCR duplicates removed. Aligned reads were then paired and filtered for fragments containing ligations of at least two different restriction fragments. These reads were then binned at 5-kb resolution. To generate the contact matrix at multiple resolutions (5, 10, 25, 40, 50, 100, 250, 500 kb, 1, 2.5, 5, and 10 Mb), we used the run-cool2multirescool script from 4DN consortium, which performed the ICE normalization at the same time. We used coolbox to visualize ICE normalized genomic HiC data. Juicer tool was also used to generate multiresolution .hic files, which can be visualized using Juicebox.

In Figure 1, we divided the whole genome into 60,000 bins at 50kb resolution and grouped them based on the enrichment of DHS domains. We have previously analyzed DHS-seq datasets from 78 different cell types in the ENCODE database[15], which identified 0.8 million open chromatin domains (DHS domains) and defined a series of categories of DHS domains based on their chromatin accessibility and histone modification data. Here, in this study we aligned the PCA values derived from HiC contact intensities with the domain categories.

To study DEX induced chromatin conformation changes on a genome-wide scale, we compared HiC contact intensities before and after DEX treatment in ALL-54S and ALL-50R, and defined dynamic bins and stable bins as described in the legend of Figure 1D. To further interrogate the subset of stable bins, we divided these regions into those with high (-0.2 < PCA < 0.2 and values of each group > 0) and low (-0.2 < PCA < 0.2 and values of each group < 0) contact intensities. Next, ΔΔHiC was calculated as ΔHiC of ALL-54S (DEX − Control) - ΔHiC of ALL-50R (DEX − Control), which depicts differential bin activity between control and dexamethasone-treated group in ALL-50R and -54S following dexamethasone treatment *in vivo*. ΔΔHiC Fold change < -0.24 or > 0.24 and $-\log_{10}$ (adj.p-Value) > 0.2 were considered as significant changed bins.

## RNA-seq and ChIP-seq Data Analysis

RNA-seq and ChIP-seq analyses were performed as previously described[72], in brief: sequencing reads were aligned to human genome (hg19) using the Burrows-Wheeler Aligner (BWA, default parameters)[73] and visualized using the UCSC Genome Browser. Peak calling was performed using three peak calling algorithms, HOMER (REF, FDR 1e-3 and 1e-2)[35], MACS[74] (p < 1e-5 and p < 1e-9) and SPP[75] (FDR 1e-2 and FDR 1e-5). Peaks identified by two or more of these algorithms were kept in the final peak list. These sites were assigned as regulatory regions to specific genes using the genomic regions enrichment of annotations tool (GREAT) analysis package[76].

Paired end RNA sequencing reads were aligned to the human genome (hg19) using the software STAR (v2.5.0b)[77] with standard parameters. Gene expression levels were quantified using htseq (v0.9)[78] and TMM normalized using the software package DESeq (v3.6) in the R statistical analysis software (v3.3.3)[79,80]. Signal intensity of the regulatory regions was defined by normalizing absolute reads of each peak to total reads of the dataset and region size. Heatmaps of gene expression profiles and epigenetic profiles at related regulatory regions were generated using Genepattern (Broad Institute, USA). Hierarchical clustering was performed using the commercially available package Partek Genomics Suite (version 6.6). The RNA-seq, ChIP-seq, and HiC data have been deposited in NCBI's Gene Expression Omnibus (GSE109949 and GSE236085).

## Link Enhancer with Promoter Using HiC Data

To map enhancer with promoter using HiC data, interaction normalization, matrix creation, significant interaction identification at 10-kb resolution were performed by using HOMER tools (v4.11.1)[81]. Gene annotations (version GeneCode V42lift37) were retrieved from UCSC[82,83]. Gene TSS regions that are upstream or downstream 1.5 kb of the interactions of GR binding LSOs are extracted based on the significant interactions of the HiC data. Interacting pairs were deduplicated and sorted by HiC scores.

## Co-binding Z-Score Calculation

The bootstrapping technique described in our previous publication[37] was used to assess the statistical significance of combinatorial binding events involving CTCF, EBF1, PU.1 and GR across all 15 potential binding patterns. In brief, we used a conservative estimate of 80,000 binding sites per protein as described before[84,85] to establish a background distribution of combinatorial binding events and then calculated a standardized z-score to measure the deviation between the number of combinatorial binding events (i.e., determined by ChIP-Seq) from the expected mean of the background distribution.

## Motif Analysis

Motif analyses were performed based on ChIP-seq data of H3K4Me1, H3K27Ac, H3K4Me3, H3K27Me3 and GR in ALL-50R and -54S before and post DEX treatment in PDX models *in vivo*. As defined in Figure 4, GR-bound regulatory domains were stratified into 15 categories, i.e., (1) promoters (Pro) or enhancers (Enh) are marked by H3K4Me3 or H3K4Me1, respectively (S); (2) transcriptionally active (A) regions are marked by H3K27Ac; (3) repressed (R) regions are marked by H3K27Me3; (4) bivalent regions (Bi) are marked by H3K27Ac and H3K27Me3; and (5) regions lacking any ChIP enrichment are defined as no signal (NS). Next, GR-bound regions matching the following criteria were selected (**Table S4**)

1. defined as Pro-S or Pr-Enh-S or RO or NS in ALL-50R control, **AND**
2. defined as Pro-S or Pr-Enh-S or RO or NS in DEX-treated ALL-50R, **AND**
3. defined as Pro-S or Pr-Enh-S or RO or NS or Enh-S in ALL-54S control, **AND**
4. defined as Pro-A or Enh-A or Pro-Enh-A or AO in DEX-treated ALL-54S

The selected GR-bound regions were analyzed using an integrative genomics method for the prediction of regulatory features and cis-regulatory modules from i-cisTarget. The regulatory network model was built based on analysis of connectivity between GR, PU.1, EBF1 and TCF3 with their regulated genes by i-cisTarget and was visualized by Cytoscape.

## Motif Analysis of DB2313-Induced PU.1 Loss

The extended "DB-sensitive" PU.1 motif (derived from examination of DB2115 displaced PU.1 binding in MOLM13 cells from Taylor et al., under review[46]) was used to calculate a log-odds score for GR-LSOs and non-GR-LSOs using the annotate peaks function from the Homer package with the -m and -mscore options enabled[35].

## Luciferase Reporter Assays

Sequences of target regulatory elements were synthesized as dsDNA by Integrated DNA Technologies (Coralville, IA, USA) and inserted into pGL3-promoter (pGL3p) vector (Promega, Madison, Wisconsin, USA) between Sal1 and BamH1 cutting sites downstream of the firefly luciferase gene. The cloned vector was co-transfected with pRL-TK renilla luciferase control reporter vectors (Promega) into Nalm6 cells. The firefly and renilla luminescence were detected in the transfected cells treated with DB2313 (MCE, NJ, USA) in the presence or absence of DEX (Sigma) using the Dual-Glo Luciferase Assay System (Promega). The firefly luminescence was normalized to renilla luminescence for each condition. Fold inductions were then calculated by normalizing to pGL3p control.

## Cytotoxicity Assays

Nalm6 cell line was cultured in RPMI 1640 media supplemented with 10% FCS, 1 mmol/L pyruvate, nonessential amino acids, 10 mmol/L 2-mercaptoethanol, and 2 mmol/L L-glutamine. Nalm6 cells were seeded in 96-well U bottomed plates at 20000 cells per 100 μL medium per well. DB2313 or vehicle control was added to a final concentration of 1 μM in triplicate wells. After 48 hr, 10 μM DEX (Sigma) or vehicle control was added to the cells pre-treated with either DB2313 or vehicle control. The cells were incubated for a series of time points. Following the incubation, Cell Counting Kit-8 (Vazyme) was added. After an additional 4 hr incubation, fluorescence was measured (450 nm) and cell viability expressed relative to vehicle-treated control cells. The presumed additive effect of combination treatment (DB2313 and DEX) was

shown by viability% of DB2313 × viability% of DEX-treated conditions. Synergy score was calculated as by SynergyFinder (https://synergyfinder.fimm.fi). The p values were calculated as the combination vs. the presumed additive effect at each concentration point.

## qRT-PCR

Quantitative real time polymerase chain reaction (qRT-PCR) was carried out as previously described[15,25]. Briefly, total RNA was isolated using TRIzol (life technologies) and cDNA was synthesized using HiScriptIII All-in-one RT SuperMix kit (Vazyme). Primers and probes for targeted genes were purchased from Life Technologies and qRT-PCR was carried out in triplicate under cycling conditions according to the manufacturer's instructions. qRT-PCR was conducted using the ChamQ Universal SYBR qPCR Master Mix (Vazyme) on a ViiA 7 qRT-PCR system (Applied Biosystems, Waltham, MA). Relative expression of target genes was calculated using glyceraldehyde-3-phosphate dehydrogenase (GAPDH) expression as control. The sequences of primers used are as follows:

- *BIM*        forward primer, '5-TAAGTTCTGAGTGTGACCGAGA-3'

reverse primer, '5-GCTCTGTCTGTAGGGAGGTAGG-3';

- *RASA1*         forward primer, '5-ACTTGACAGAACGATAGCAGAAG-3'

reverse primer '5-GCCTCCGATCACTCTCTCTTA-3';

- *ZBTB16*       forward primer, '5-GAGATCCTCTTCCACCGCAAT-3'

reverse primer '5-CCGCATACAGCAGGTCATC-3';

- *GliZ*         forward primer, '5-AACACCGAAATGTATCAGACCC-3'

reverse primer, '5-TGTCCAGCTTAACGGAAACCA-3';

- *GAPDH*       forward primer, '5-GGAGCGAGATCCCTCCAAAAT-3'

reverse primer, '5-GGCTGTTGTCATACTTCTCATGG-3'.

## CRISPR/Cas9-Mediated *In Vivo* Gene Knockout (KO)

Stable Cas9-expressing PDX cells were generated using the FU-Cas9-mCherry plasmid (Addgene #70182). In brief, HEK293FT cells (Invitrogen) were transfected using Lipofectamine™ 2000 (Thermo Fisher Scientific 11668019) with FU-CAS9-mCherry and the pMD2.G envelope (Addgene #12259) and psPAX2 packaging plasmids (Addgene #12260) to generate lentiviral particles. PDX cells were revived and transduced *ex vivo* with lentivirus for 24 hours, washed in PBS and injected into NSG mice (Australian Bioresources) for *in vivo* expansion (1 million cells per mouse). Mice were sacrificed at high leukemia burden (>50% huCD45+% in mouse peripheral blood) and PDX cells harvested from the spleen. mCherry+ cells were sorted by fluorescence-activated cell sorting (FACS) to generate a purified Cas9-mCherry population and reinjected into naïve NSG mice for *in vivo* expansion.

For gene KO, single guide RNA (sgRNA) sequences against human *SPI1 (PU.1), BCL2L11 (BIM)* or non-targeting sgRNA sequences were cloned into the FgH1tUTG (Addgene #70138) GFP vector and lentiviral particles made as described above. Cas9-mCherry+ PDX cells were transduced, *in vivo* expanded, and sorted by FACS to generate a purified mCherry+ GFP+ population and reinjected into naïve NSG mice for *in vivo* expansion. sgRNA sequences are as follows:

| Targeted Genes | sgRNA sequence |
| --- | --- |
| *SPI1* | AATACTCGTGCGTTTGGCGT |
| *BCL2L11* | GCCCAAGAGTTGCGGCGTAT |
| Human non-targeting sequence | ACGGAGGCTAAGCGTCGCAA |

For *in vivo* gene KO and drug efficacy testing, Cas9-mCherry+ sgRNA-GFP+ PDX cells were injected into NSG mice (6 mice/treatment group) and mice switched to Doxycycline-impregnated food (600mg/kg Doxycycline) 7 days post-injection to activate sgRNA expression. Leukemia level was tracked weekly by tail vein bleeding and quantifying huCD45+ cells in mouse peripheral blood. At 1% huCD45+, DEX treatment was administered via intraperitoneal injection at 15mg/kg daily, 5 days on/2 days off for 4 weeks. A leukemia event is defined as 25% huCD45+, or when the animal is euthanised due to leukemia-related morbidity, and event-free survival (EFS) was used to assess therapeutic enhancement

with statistical significance defined as p<0.01. At leukemia event, mice were sacrificed and PDX cells harvested from the spleen for quantification of CRISPR efficiency.

### Evaluation of Indel Mutagenesis

The CRISPR/Cas9-induced indel frequencies were quantified by Tracking of Indels by Decomposition (TIDE) [86]. Genomic DNA was extracted using Isolate II Genomic DNA Kit (Bioline BIO-52066) following manufacturer's instructions. 100 ng genomic DNA was PCR amplified using Q5 polymerase (NEB M0494X) and primers flanking the sgRNA target region. The PCR products are next subjected to standard Sanger sequencing and the sequence data files of the edited samples and the wild-type samples were analyzed by the TIDE webtool (http://tide.nki.nl). Primer sequences used for INDEL quantification by TIDE assay are as follows:

| Genes | Forward primer (5'-3') | Reverse primer (5'-3') |
|---|---|---|
| *SPI1* | GGAAGAAATGAACCCCGCAC | GAGGGCTGTAGGTCCAACG |
| *BCL2L11* | GGTTGGAATGTTTTCAGTTCTTGC | TCCTTTGCTGCCTCCTACTG |

### Protein Structure Analysis

Mutated PU.1 proteins structures were predicted using Aphafold2 [47] based on the following amino acid sequences and the results were viewed with PyMOL.

- Mutant #1: Serine insertion

MLQACKMEGFPLVPPQPSEDLVPYDTDLYQR_S_QTHEYYPYLSSDGESHSDHYWDFHPHHVHSEFESFAENNFTELQSVQPPQ LQQLYRHMELEQMHVLDTPMVPPHPSLGHQVSYLPRMCLQYPSLSPAQPSSDEEEGERQSPPLEVSDGEADGLEPGPGLLPGETGSKKKIRL YQFLLDLLRSGDMKDSIWWVDKDKGTFQFSSKHKEALAHRWGIQKGNRKKMTYQKMARALRNYGKTGEVKKVKKKLTYQFSGEVLGRGGLAERRHPPH

- Mutant #2: Glycine and Valine insertion

MLQACKMEGFPLVPPQPSEDLVPYDTDLYQR_GV_QTHEYYPYLSSDGESHSDHYWDFHPHHVHSEFESFAENNFTELQSVQPPQLQ QLYRHMELEQMHVLDTPMVPPHPSLGHQVSYLPRMCLQYPSLSPAQPSSDEEEGERQSPPLEVSDGEADGLEPGPGLLPGETGSKKKIRL YQFLLDLLRSGDMKDSIWWVDKDKGTFQFSSKHKEALAHRWGIQKGNRKKMTYQKMARALRNYGKTGEVKKVKKKLTYQFSGEVLGRGGLAERRHPPH

### Quantification and Statistical Analysis

HiC-seq, RNA-seq and ChIP-seq studies were performed using PDX cells from three randomized ALL-engrafted mice at each condition of treatments. Gene expression and cytotoxicity studies were performed with three independent experiments. Quantitative variables of normally distributed data were compared by the student *t* test and non-normally distributed data were compared by the Mann-Whitney *U* test. All statistical tests were two-sided and p values <0.05 were considered statistically significant.

### Data and Software Availability

The datasets generated and/or analyzed in this study are deposited in the NCBI's Gene Expression Omnibus repository (GSE109949 and GSE236085). The GSE109949 is publicly available and the GSE236085 can be accessed with a token mravgggutfcpfsv. We also host a UCSC genome browser session for easy access and viewing of genome-wide mapping at:

- https://www.genome.ucsc.edu/s/Sally%20Cao/All%20peaks%20%2D%20NC

## Declarations

## Author information

These authors contributed equally: Dominik Beck, Honghui Cao, Feng Tian, Yizhou Huang

### Authors and Affiliations

**Shanghai Institute of Hematology, State Key Laboratory of Medical Genomics, National Research Center for Translational Medicine at Shanghai, Ruijin Hospital Affiliated to Shanghai Jiao Tong University School of Medicine, Shanghai, China**

Honghui Cao, Han Zhao, Wenqian Xu[1], Gaoxian Song[1], Jin Wang[1], Jian-Qing Mi[1], Duohui Jing

**Centre for Health Technologies and the School of Biomedical Engineering, University of Technology, Sydney, Australia**

Dominik Beck, Diego Chacon-Fajardo

**School of Medicine, Hebei University of Engineering, Handan, Hebei Province, China**

Feng Tian

**Children's Cancer Institute, Lowy Cancer Research Centre, School of Clinical Medicine, UNSW Medicine & Health, UNSW Centre for Childhood Cancer Research, UNSW Sydney, Sydney, Australia**

Yizhou Huang, Hansen J Kosasih, Yashna Walia, Richard B Lock, Charles E. de Bock

**Department of Plastic and Reconstructive Surgery, Shanghai Ninth People's Hospital, Shanghai Jiao Tong University School of Medicine, Shanghai, China**

Xiaolu Tai, Meng Wang, Chao Zhang

**Centre for Blood Research, University of York, United Kingdom**

David J Kealy, Katherine S Bridge

**York Biomedical Research Institute, University of York, United Kingdom**

Weiye Zhao, Andrew N Holding

**Metabolomics & Proteomics Laboratory, Bioscience Technology Facility, Department of Biology, University of York, United Kingdom**

Adam A Dowle

**Department of Cell Biology, Albert Einstein College of Medicine, Bronx, USA**

Samuel J Taylor

## Authorship Contributions

DJ, DB, RBL and CEB designed the study. DJ, HC, YH, XT, HJK, DJK, KSB, WZ, ANH and AADperformed experiments and analyzed the data. DB and FT performed bioinformatics analysis. DJ, DB, HC, CEB and RBL interpreted the data and wrote the manuscript. HZ, WX, GS and MW assisted in performing experiments and data analysis. DCF, YW and SJT contributed to bioinformatics analysis. CZ, JW and JQM contributed to the data interpretation and revision of the manuscript.

## Corresponding author

Correspondence to Dominik Beck, Richard B Lock, Charles E. de Bock, Duohui Jing

## Competing interests

The authors declare no conflict of interests.

# References

1. Kim, I.K., *et al.* Glucocorticoid-induced tumor necrosis factor receptor-related protein co-stimulation facilitates tumor regression by inducing IL-9-producing helper T cells. *Nat Med* **21**, 1010-1017 (2015).

2. Palumbo, A., *et al.* Daratumumab, bortezomib, and dexamethasone for multiple myeloma. *N Engl J Med* **375**, 754-766 (2016).

3. Bhojwani, D. & Pui, C.H. Relapsed childhood acute lymphoblastic leukaemia. *Lancet Oncol* **14**, e205-217 (2013).

4. Pui, C.H. & Evans, W.E. A 50-year journey to cure childhood acute lymphoblastic leukemia. *Semin Hematol* **50**, 185-196 (2013).

5. Hunger, S.P. & Mulligan, C.G. Acute lymphoblastic leukemia in children. *N Engl J Med* **373**, 1541-1552 (2015).

6. Klein, K., *et al.* Glucocorticoid-induced proliferation in untreated pediatric acute myeloid leukemic blasts. *Pediatr Blood Cancer* **63**, 1457-1460 (2016).

7. Gruver-Yates, A.L. & Cidlowski, J.A. Tissue-specific actions of glucocorticoids on apoptosis: a double-edged sword. *Cells* **2**, 202-223 (2013).

8. Cain, D.W. & Cidlowski, J.A. Immune regulation by glucocorticoids. *Nat Rev Immunol* **17**, 233-247 (2017).

9. Watson, L.C., *et al.* The glucocorticoid receptor dimer interface allosterically transmits sequence-specific DNA signals. *Nat Struct Mol Biol* **20**, 876-883 (2013).

10. Vockley, C.M., *et al.* Direct GR binding sites potentiate clusters of TF binding across the human genome. *Cell* **166**, 1269-1281 e1219 (2016).

11. Guo, B., Huang, X., Cooper, S. & Broxmeyer, H.E. Glucocorticoid hormone-induced chromatin remodeling enhances human hematopoietic stem cell homing and engraftment. *Nat Med* **23**, 424-428 (2017).

12. Swinstead, E.E., *et al.* Steroid receptors reprogram FoxA1 occupancy through dynamic chromatin transitions. *Cell* **165**, 593-605 (2016).

13. Aranda, S., Mas, G. & Di Croce, L. Regulation of gene transcription by Polycomb proteins. *Sci Adv* **1**, e1500737 (2015).

14. Hnisz, D., Day, D.S. & Young, R.A. Insulated neighborhoods: structural and functional units of mammalian gene control. *Cell* **167**, 1188-1200 (2016).

15. Jing, D., *et al.* Lymphocyte-Specific Chromatin Accessibility Pre-determines Glucocorticoid Resistance in Acute Lymphoblastic Leukemia. *Cancer Cell* **34**, 906-921 e908 (2018).

16. Bergeron, B.P., *et al.* Epigenomic profiling of glucocorticoid responses identifies cis-regulatory disruptions impacting steroid resistance in childhood acute lymphoblastic leukemia. *Leukemia* **36**, 2374-2383 (2022).

17. Krivtsov, A.V., *et al.* A Menin-MLL Inhibitor Induces Specific Chromatin Changes and Eradicates Disease in Models of MLL-Rearranged Leukemia. *Cancer Cell* **36**, 660-673 e611 (2019).

18. Li, J., *et al.* PRC2 Inhibitors Overcome Glucocorticoid Resistance Driven by NSD2 Mutation in Pediatric Acute Lymphoblastic Leukemia. *Cancer discovery* (2021).

19. Liu, Y.F., *et al.* Genomic Profiling of Adult and Pediatric B-cell Acute Lymphoblastic Leukemia. *EBioMedicine* **8**, 173-183 (2016).

20. Li, J.F., *et al.* Transcriptional landscape of B cell precursor acute lymphoblastic leukemia based on an international study of 1,223 cases. *Proceedings of the National Academy of Sciences of the United States of America* **115**, E11711-E11720 (2018).

21. El-Hoss, J., *et al.* A single nucleotide polymorphism genotyping platform for the authentication of patient derived xenografts. *Oncotarget* **7**, 60475-60490 (2016).

22. Liem, N.L., *et al.* Characterization of childhood acute lymphoblastic leukemia xenograft models for the preclinical evaluation of new therapies. *Blood* **103**, 3905-3914 (2004).

23. Bachmann, P.S., *et al.* Divergent mechanisms of glucocorticoid resistance in experimental models of pediatric acute lymphoblastic leukemia. *Cancer Res* **67**, 4482-4490 (2007).

24. Lee, E.M., *et al.* Efficacy of an Fc-modified anti-CD123 antibody (CSL362) combined with chemotherapy in xenograft models of acute myelogenous leukemia in immunodeficient mice. *Haematologica* **100**, 914-926 (2015).

25. Jing, D., *et al.* Opposing regulation of BIM and BCL2 controls glucocorticoid-induced apoptosis of pediatric acute lymphoblastic leukemia cells. *Blood* **125**, 273-283 (2015).

26. Jones, L., *et al.* A review of new agents evaluated against pediatric acute lymphoblastic leukemia by the Pediatric Preclinical Testing Program. *Leukemia* **30**, 2133-2141 (2016).

27. Jin, L., *et al.* Monoclonal antibody-mediated targeting of CD123, IL-3 receptor alpha chain, eliminates human acute myeloid leukemic stem cells. *Cell Stem Cell* **5**, 31-42 (2009).

28. Piovan, E., *et al.* Direct reversal of glucocorticoid resistance by AKT inhibition in acute lymphoblastic leukemia. *Cancer Cell* **24**, 766-776 (2013).

29. van Galen, J.C., *et al.* BTG1 regulates glucocorticoid receptor autoinduction in acute lymphoblastic leukemia. *Blood* **115**, 4810-4819 (2010).

30. Jones, C.L., *et al.* MAPK signaling cascades mediate distinct glucocorticoid resistance mechanisms in pediatric leukemia. *Blood* **126**, 2202-2212 (2015).

31. Serafin, V., *et al.* Glucocorticoid resistance is reverted by LCK inhibition in pediatric T-cell acute lymphoblastic leukemia. *Blood* **130**, 2750-2761 (2017).

32. Nagao, K., Iwai, Y. & Miyashita, T. RCAN1 is an important mediator of glucocorticoid-induced apoptosis in human leukemic cells. *PLoS One* **7**, e49926 (2012).

33. Cialfi, S., *et al.* Glucocorticoid sensitivity of T-cell lymphoblastic leukemia/lymphoma is associated with glucocorticoid receptor-mediated inhibition of Notch1 expression. *Leukemia* **27**, 485-488 (2013).

34. Boller, S., Li, R. & Grosschedl, R. Defining B cell chromatin: lessons from EBF1. *Trends Genet* **34**, 257-269 (2018).

35. Heinz, S., *et al.* Simple combinations of lineage-determining transcription factors prime cis-regulatory elements required for macrophage and B cell identities. *Mol Cell* **38**, 576-589 (2010).

36. de la Rica, L., *et al.* PU.1 target genes undergo Tet2-coupled demethylation and DNMT3b-mediated methylation in monocyte-to-osteoclast differentiation. *Genome Biol* **14**, R99 (2013).

37. Beck, D., *et al.* Genome-wide analysis of transcriptional regulators in human HSPCs reveals a densely interconnected network of coding and noncoding genes. *Blood* **122**, e12-22 (2013).

38. Corces, M.R., *et al.* Lineage-specific and single-cell chromatin accessibility charts human hematopoiesis and leukemia evolution. *Nat Genet* **48**, 1193-1203 (2016).

39. Dekker, J., *et al.* The 4D nucleome project. *Nature* **549**, 219-226 (2017).

40. Imrichova, H., Hulselmans, G., Atak, Z.K., Potier, D. & Aerts, S. i-cisTarget 2015 update: generalized cis-regulatory enrichment analysis in human, mouse and fly. *Nucleic Acids Res* **43**, W57-64 (2015).

41. Herrmann, C., Van de Sande, B., Potier, D. & Aerts, S. i-cisTarget: an integrative genomics method for the prediction of regulatory features and cis-regulatory modules. *Nucleic Acids Res* **40**, e114 (2012).

42. Papachristou, E.K., *et al.* A quantitative mass spectrometry-based approach to monitor the dynamics of endogenous chromatin-associated protein complexes. *Nat Commun* **9**, 2311 (2018).

43. Shannon, P., *et al.* Cytoscape: a software environment for integrated models of biomolecular interaction networks. *Genome Res* **13**, 2498-2504 (2003).

44. Savage, A.K., *et al.* The transcription factor PLZF directs the effector program of the NKT cell lineage. *Immunity* **29**, 391-403 (2008).

45. Whyte, W.A., *et al.* Master transcription factors and mediator establish super-enhancers at key cell identity genes. *Cell* **153**, 307-319 (2013).

46. Taylor, S., *et al.* Transcription Factor Redistributors Pharmacologically Actuate Non-Canonical Gene Networks to Drive AML Differentiation. *Blood* **142**, 119-119 (2023).

47. Jumper, J., *et al.* Highly accurate protein structure prediction with AlphaFold. *Nature* **596**, 583-589 (2021).

48. Quatrini, L. & Ugolini, S. New insights into the cell- and tissue-specificity of glucocorticoid actions. *Cell Mol Immunol* **18**, 269-278 (2021).

49. Bachmann, P.S., Gorman, R., Mackenzie, K.L., Lutze-Mann, L. & Lock, R.B. Dexamethasone resistance in B-cell precursor childhood acute lymphoblastic leukemia occurs downstream of ligand-induced nuclear translocation of the glucocorticoid receptor. *Blood* **105**, 2519-2526 (2005).

50. Bachmann, P.S., *et al.* Epigenetic silencing of BIM in glucocorticoid poor-responsive pediatric acute lymphoblastic leukemia, and its reversal by histone deacetylase inhibition. *Blood* **116**, 3013-3022 (2010).

51. Bonnet, D. & Dick, J.E. Human acute myeloid leukemia is organized as a hierarchy that originates from a primitive hematopoietic cell. *Nature medicine* **3**, 730-737 (1997).

52. Visvader, J.E. & Lindeman, G.J. Cancer stem cells in solid tumours: accumulating evidence and unresolved questions. *Nat Rev Cancer* **8**, 755-768 (2008).

53. Essers, M.A. & Trumpp, A. Targeting leukemic stem cells by breaking their dormancy. *Molecular oncology***4**, 443-450 (2010).

54. Kong, Y*., et al.* CD34+CD38+CD19+ as well as CD34+CD38-CD19+ cells are leukemia-initiating cells with self-renewal capacity in human B-precursor ALL. *Leukemia***22**, 1207-1213 (2008).

55. le Viseur, C*., et al.* In childhood acute lymphoblastic leukemia, blasts at different stages of immunophenotypic maturation have stem cell properties. *Cancer Cell***14**, 47-58 (2008).

56. Rehe, K*., et al.* Acute B lymphoblastic leukaemia-propagating cells are present at high frequency in diverse lymphoblast populations. *EMBO Mol Med***5**, 38-51 (2013).

57. Spinella, J.F*., et al.* Mutational dynamics of early and late relapsed childhood ALL: rapid clonal expansion and long-term dormancy. *Blood Adv***2**, 177-188 (2018).

58. Ma, X*., et al.* Rise and fall of subclones from diagnosis to relapse in pediatric B-acute lymphoblastic leukaemia. *Nat Commun***6**, 6604 (2015).

59. Kim, J.C*., et al.* Transcriptomic classes of BCR-ABL1 lymphoblastic leukemia. *Nat Genet* (2023).

60. Johnstone, S.E*., et al.* Large-Scale Topological Changes Restrain Malignant Progression in Colorectal Cancer. *Cell***182**, 1474-1489 e1423 (2020).

61. Kloetgen, A*., et al.* Three-dimensional chromatin landscapes in T cell acute lymphoblastic leukemia. *Nat Genet***52**, 388-400 (2020).

62. Xu, J*., et al.* Subtype-specific 3D genome alteration in acute myeloid leukaemia. *Nature***611**, 387-398 (2022).

63. Schuetzmann, D*., et al.* Temporal autoregulation during human PU.1 locus SubTAD formation. *Blood***132**, 2643-2655 (2018).

64. Constantinides, M.G. & Belkaid, Y. Early-life imprinting of unconventional T cells and tissue homeostasis. *Science***374**, eabf0095 (2021).

65. Kosan, C*., et al.* Transcription factor miz-1 is required to regulate interleukin-7 receptor signaling at early commitment stages of B cell differentiation. *Immunity***33**, 917-928 (2010).

66. Chen, Z*., et al.* Fusion between a novel Krüppel-like zinc finger gene and the retinoic acid receptor-alpha locus due to a variant t(11;17) translocation associated with acute promyelocytic leukaemia. *Embo j***12**, 1161-1167 (1993).

67. Chen, B*., et al.* Identification of fusion genes and characterization of transcriptome features in T-cell acute lymphoblastic leukemia. *Proceedings of the National Academy of Sciences of the United States of America***115**, 373-378 (2018).

68. Dai, Y.T*., et al.* Transcriptome-wide subtyping of pediatric and adult T cell acute lymphoblastic leukemia in an international study of 707 cases. *Proceedings of the National Academy of Sciences of the United States of America***119**, e2120787119 (2022).

69. Mohammed, H*., et al.* Rapid immunoprecipitation mass spectrometry of endogenous proteins (RIME) for analysis of chromatin complexes. *Nature protocols***11**, 316-326 (2016).

70. Demichev, V., Messner, C.B., Vernardis, S.I., Lilley, K.S. & Ralser, M. DIA-NN: neural networks and interference correction enable deep proteome coverage in high throughput. *Nature methods***17**, 41-44 (2020).

71. Belaghzal, H., Dekker, J. & Gibcus, J.H. Hi-C 2.0: An optimized Hi-C procedure for high-resolution genome-wide mapping of chromosome conformation. *Methods***123**, 56-65 (2017).

72. Chacon, D., Beck, D., Perera, D., Wong, J.W. & Pimanda, J.E. BloodChIP: a database of comparative genome-wide transcription factor binding profiles in human blood cells. *Nucleic Acids Res***42**, D172-177 (2014).

73. Li, H. & Durbin, R. Fast and accurate short read alignment with Burrows-Wheeler transform. *Bioinformatics***25**, 1754-1760 (2009).

74. Zhang, Y*., et al.* Model-based analysis of ChIP-Seq (MACS). *Genome Biol***9**, R137 (2008).

75. Kharchenko, P.V., Tolstorukov, M.Y. & Park, P.J. Design and analysis of ChIP-seq experiments for DNA-binding proteins. *Nat Biotechnol***26**, 1351-1359 (2008).

76. McLean, C.Y*., et al.* GREAT improves functional interpretation of cis-regulatory regions. *Nat Biotechnol***28**, 495-501 (2010).

77. Dobin, A*., et al.* STAR: ultrafast universal RNA-seq aligner. *Bioinformatics***29**, 15-21 (2013).

78. Anders, S., Pyl, P.T. & Huber, W. HTSeq–a Python framework to work with high-throughput sequencing data. *Bioinformatics***31**, 166-169 (2015).

79. McCarthy, D.J., Chen, Y. & Smyth, G.K. Differential expression analysis of multifactor RNA-Seq experiments with respect to biological variation. *Nucleic Acids Res***40**, 4288-4297 (2012).

80. Robinson, M.D., McCarthy, D.J. & Smyth, G.K. edgeR: a Bioconductor package for differential expression analysis of digital gene expression data. *Bioinformatics***26**, 139-140 (2010).

81. Lin, Y.C*., et al.* Global changes in the nuclear positioning of genes and intra- and interdomain genomic interactions that orchestrate B cell fate. *Nat Immunol***13**, 1196-1204 (2012).

82. Nassar, L.R*., et al.* The UCSC Genome Browser database: 2023 update. *Nucleic Acids Res***51**, D1188-1195 (2023).

83. Rosenbloom, K.R., *et al.* ENCODE data in the UCSC Genome Browser: year 5 update. *Nucleic Acids Res* **41**, D56-63 (2013).

84. Wilson, N.K., *et al.* Combinatorial transcriptional control in blood stem/progenitor cells: genome-wide analysis of ten major transcriptional regulators. *Cell Stem Cell* **7**, 532-544 (2010).

85. Tijssen, M.R., *et al.* Genome-wide analysis of simultaneous GATA1/2, RUNX1, FLI1, and SCL binding in megakaryocytes identifies hematopoietic regulators. *Dev Cell* **20**, 597-609 (2011).

86. Brinkman, E.K., Chen, T., Amendola, M. & van Steensel, B. Easy quantitative assessment of genome editing by sequence trace decomposition. *Nucleic Acids Res* **42**, e168 (2014).
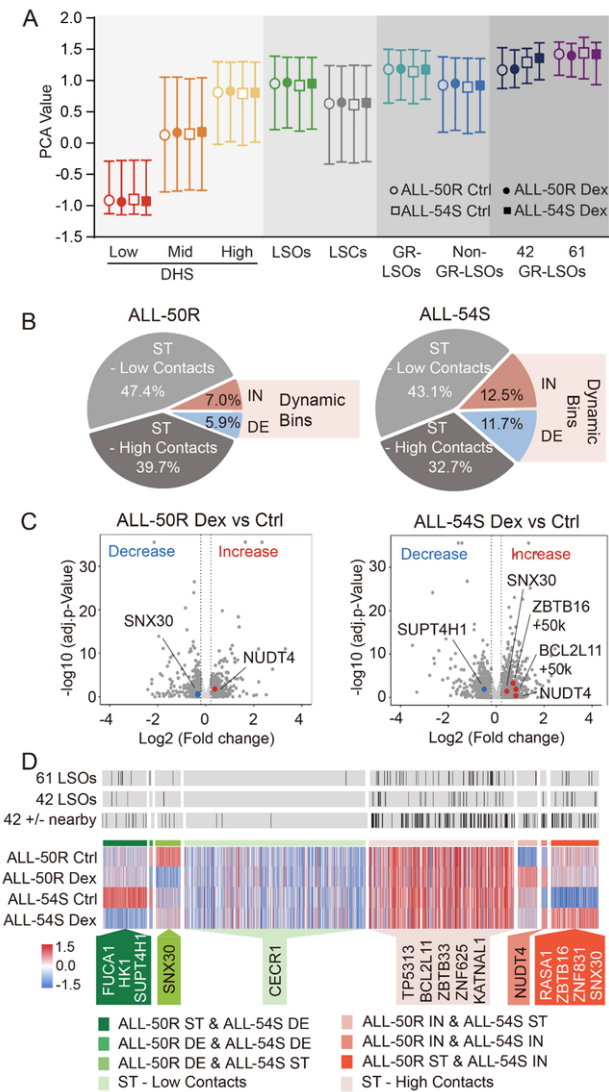
# Figures

## Figure 1



## Figure 1

**HiC multi-omics annotation and changes in ALL-54S and ALL-50R pre- and post-treatment with DEX.**

(A) HiC contact intensities were compared using principal components and visualized using boxplots. Boxplots of principal components (PCs) derived from HiC contact intensities in the following genome regions (i) 0-9 DHS domains (DHS-Low), (ii) 10-19 DHS domains (intermediate, DHS-Mid), (iii) ≧20 DHS domains (DHS-High), (iv) lymphocyte-specific open regions (LSOs), (v) lymphocyte-specific closed regions (LSCs), (vi) LSOs with GR binding (GR-LSOs), (vii) LSOs without GR binding (Non-GR-LSOs), (viii) 42 GR-LSOs with an increased H3K27Ac abundance after DEX treatment, and (ix) 61 GR-LSOs with decreased H3K27Ac abundance following DEX treatment. The bins with higher enrichments of

DHS domains exhibited more intense contacts with other regions in the genome, as indicated by the magnitude of PCA values from HiC analysis of the two ALL PDXs.

(B) HiC changes in ALL-50R and ALL-54S post-DEX treatment grouped into dynamic bins, i.e., those genome regions that increased or decreased HiC interactions (IN: negative to positive PCA values or >1.5-fold increase; DE, cutoff positive to negative PCA values or >1.5-fold decrease), and stable bins i.e., genome regions that did not change contact intensities (ST = stable, IN = increase; DE = decrease).

(C) Volcano plots depicting differential bin activity between control and dexamethasone-treated group in ALL-50R and ALL-54S following dexamethasone treatment *in vivo*.

(D) Heatmap of HiC contact intensities in ALL-50R and ALL-54S post-DEX treatment. The top row indicates the 103 (i.e., 42 GR-activated or 61 GR-repressed) LSOs as well as their adjacent bins (42 GR-LSOs +/- nearby) and the bottom row highlights genes identified by a ΔΔHiC analysis (i.e., calculated as ΔHiC of ALL-54S (Dex − Ctrl) - ΔHiC of ALL-50R (Dex − Ctrl)).

See also **Table S1-S3** and **Figure S1**.
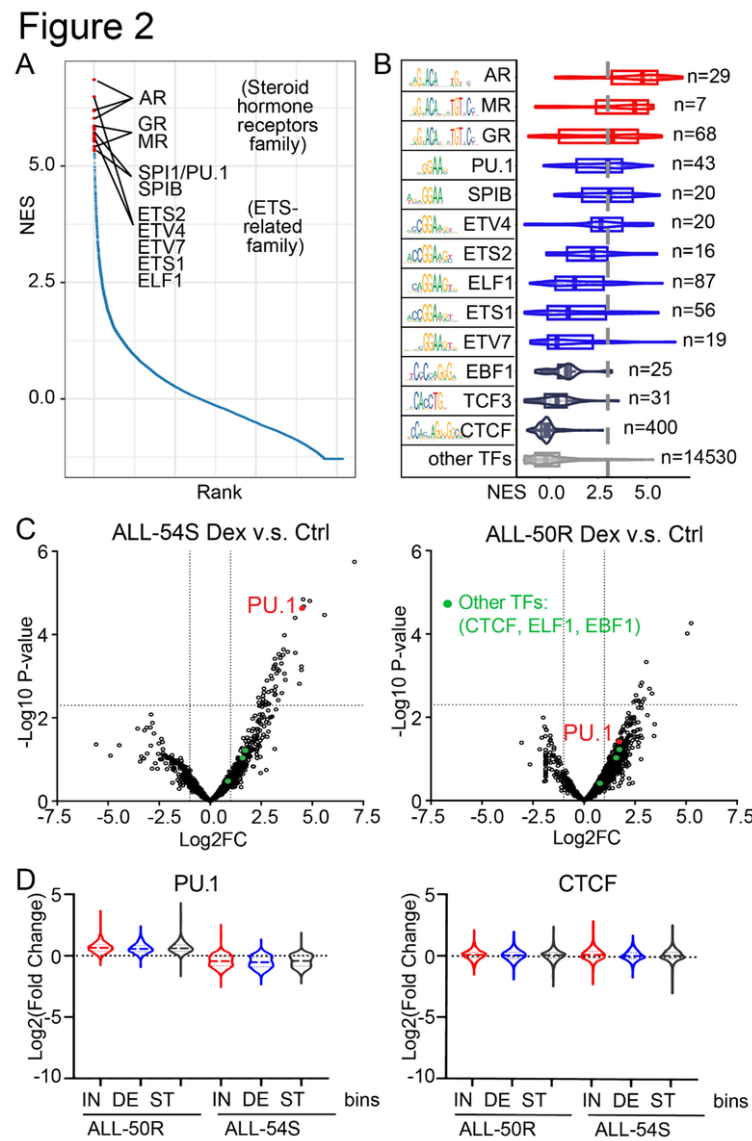
## Figure 2



Figure 2

**Identification of PU.1 as a key regulator for genome regions associated with HiC changes in ALL-54S and ALL-50R pre- and post-treatment with DEX.**

(A) Enrichment analysis using i-cisTarget to identify key regulators for genome regions associated with HiC changes in ALL-54S and ALL-50R pre- and post-treatment with DEX. The normalised enrichment score (NES) for all TFs motifs is shown in blue while the top 10 TF motifs are

highlighted in red.

(B) Violin plots of the NES for the top 10 ranked TF motifs, two lineage-specific TFs EBF1 and TCF3, and structural protein CTCF.

(C) Rapid Immunoprecipitation Mass Spectrometry (RIME) to identify proteins interacting with the GR. Interacting affinities were calculated as differential abundance of the GR-bound proteins in DEX-treated vs. control samples in ALL-50R and ALL-54S.

(D) PU.1 and CTCF ChIP-Seq enrichment contrasting ALL-50R vs ALL-54S pre- and post-treatment with DEX at regions classified as IN, DE, and ST bins as described in Figure 1B. ST =genomic bins with stable HiC-contact intensities, IN = bins with increasedHiC-contact intensities; DE = bins with decreasedHiC-contact intensities.

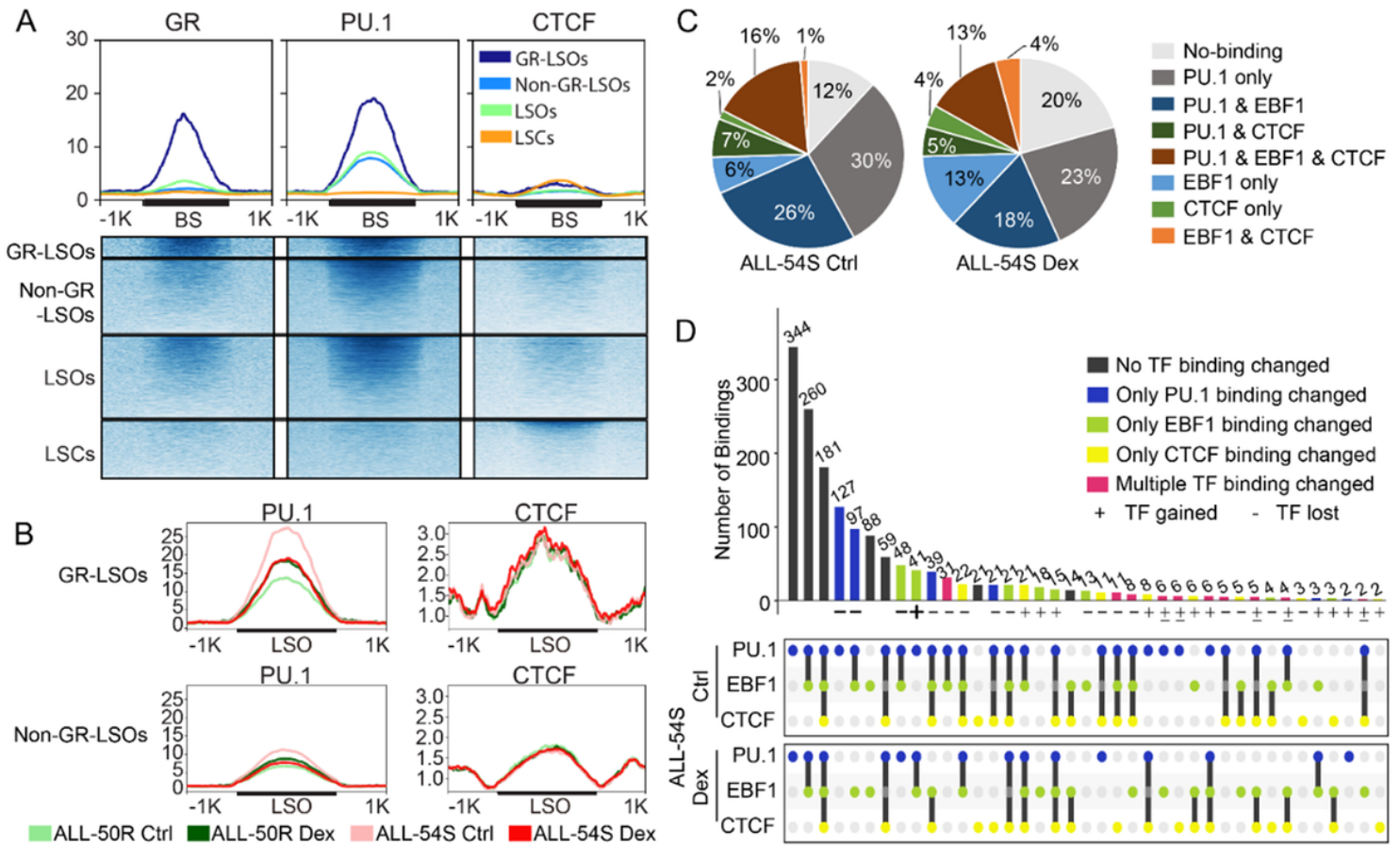See also **Table S4 and S5**

# Figure 3



Figure 3

**Combinatorial binding of PU.1 and other TFs in ALL-50R and ALL-54S pre- and post-treatment with DEX.**

(A) GR, PU.1 and CTCF ChIP-Seq profiles and heatmap plots (DeepTools) at GR-LSOs, non-GR-LSOs, LSOs and LSCs post-treatment with DEX in ALL-54S.

(B) GR, PU.1 and CTCF ChIP-Seq profile plots at GR-LSOs and non-GR-LSOs in ALL-54S and ALL-50R following treatment with DEX.

(C) Pie chart showing the co-occurrence of PU.1 with CTCF and/or EBF1 bindings in ALL-54S post-treatment with DEX.

(D) Summary of PU.1 and other TFs binding at GR-LSO in ALL-54S pre- and post-treatment with DEX.

See also **Table S6** and **Figure S2**.

# Figure 4



## Figure 4

**PU.1 binding at gene regulatory elements and associated network modules in ALL-50R and ALL-54S pre- and post-treatment with DEX.**

(A) Combinatorial code of histone modifications applied to group the epigenomes of ALL-54S and ALL-50R pre- and post-treatment with DEX: (1) promoters (Pro) or enhancers (Enh) marked by H3K4Me3 or H3K4Me1, respectively (S); (2) transcriptionally active (A) regions marked by H3K27Ac; (3) repressed (R) regions marked by H3K27Me3; (4) bivalent regions (Bi) marked by H3K27Ac and H3K27Me3; and (5) regions lacking any ChIP enrichment (NS). Lower panel: GR, CTCF and PU.1 binding at genomic regions of the categories that were defined above, in ALL-54S and ALL-50R pre- and post-treatment with DEX.

(B) Integration of RNA-Seq and ChIP-Seq at GR-LSOs and their associated genes that were identified by HiC in ALL-54S or ALL-50R. Left panel: heatmap of differentially expressed genes between ALL-54S and ALL-50R post-treatment with DEX. Right panel: heatmap and density plots (DeepTools) of H3K4Me3, H3K4Me1, H3K27Ac and H3K27Me3 ChIP-Seq profiles at the +/- 5kb regions surrounding LSOs. HiC data was used to associate LSOs with genes and the five genes with the highest scores in each LSO were used for analysis. Red box, clusters 1 and 2 showing relatively higher H3K27Ac enrichment after DEX treatment in ALL-54S; green box, genomic regions showing down-regulated H3K27Me3 enrichment in ALL-54S compared to ALL-50R.

(C) Ingenuity Pathway Analysis (IPA) identified signaling pathways (involving both activators and inhibitors) differently regulated by the GR-interacting gene (identified by RNA-seq) / protein (identified by RIME) networks in ALL-54S and ALL-50R upon dexamethasone treatment.

(D) Cystoscope model integrating i-cisTarget motifs, TF ChIP-Seq, and H3K27Ac/me3 and H3K4me1/me3 ChIP-Seq at LSOs.
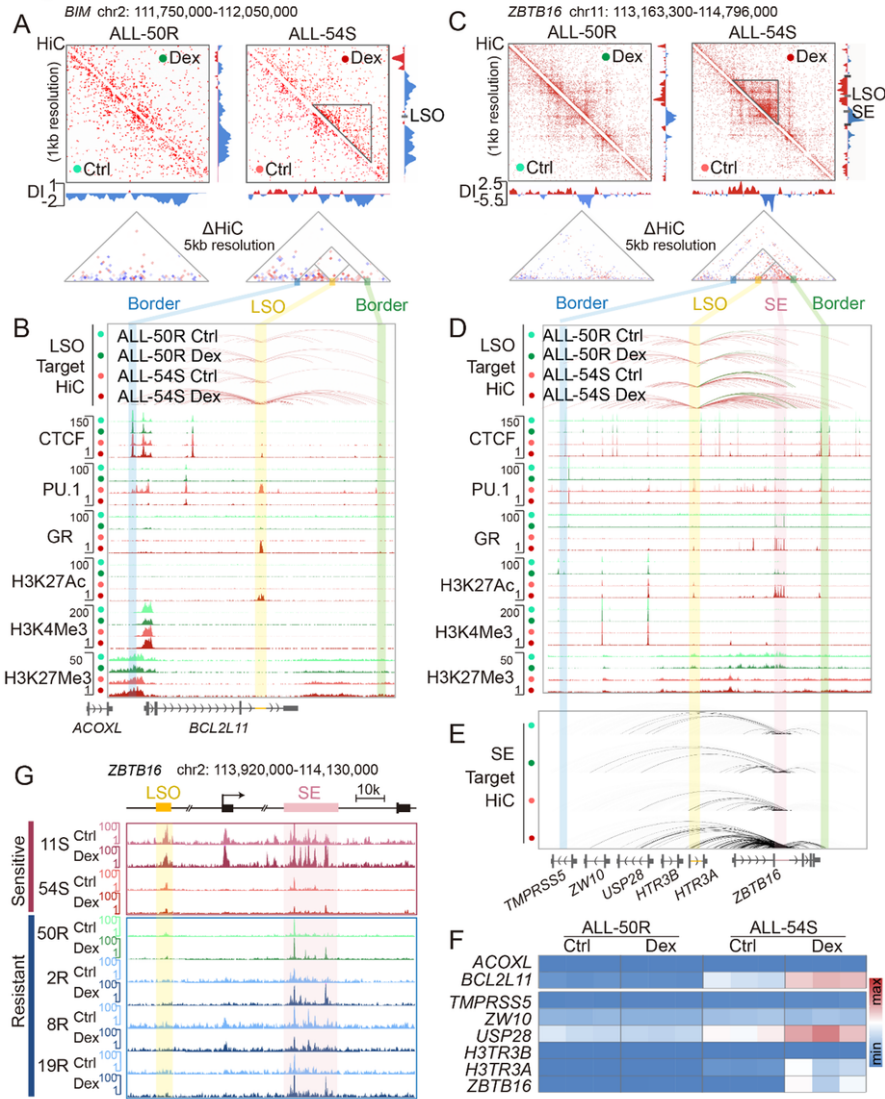
## Figure 5



### Figure 5

**Multi-omics annotation of two *de novo* TADs at the *BIM* and *ZBTB16* loci in ALL-50R and ALL-54S pre- and post-treatment with DEX.**

(A) HiC interaction map and ΔHiC analysis at the *BIM* TAD ALL-54S and ALL-50R pre- and post-treatment with DEX (top) and directionality index (DI; bottom). DI shows a preference to interact with either an up or downstream region. Triangles indicate TADs.

(B) UCSC Genome Browser tracks at the *BIM* locus showing data from (i) LSO-Target HiC showing genomic regions interacting with the *BIM* LSO, (ii) CTCF, PU.1 and GR ChIP-Seq, and (iii) H3K27Ac, H3K4Me1, and H3K27Me3 ChIP-Seq. Highlighted in blue and green are the up and downstream TAD borders, and in yellow the LSO.

(C) Same as (A) but for *ZBTB16*. (D) Same as (B) but for *ZBTB16.*

(*E*) UCSC Genome Browser tracks of SE-Target HiC showing all genomic regions interacting with the *ZBTB16* super enhancer (SE).

(F) Heatmaps show RNA-seq data of gene expression within the *BCL2L11 (BIM)* TAD and *ZBTB16* TAD in ALL-50R and -54S following dexamethasone administration *in vivo*. Ctrl, control. Dex, dexamethasone.

(G) ATAC-seq analysis showing accessible genomic regions at the *ZBTB16* locus in a panel of sensitive and resistant ALL PDXs pre- and post-treatment with DEX.
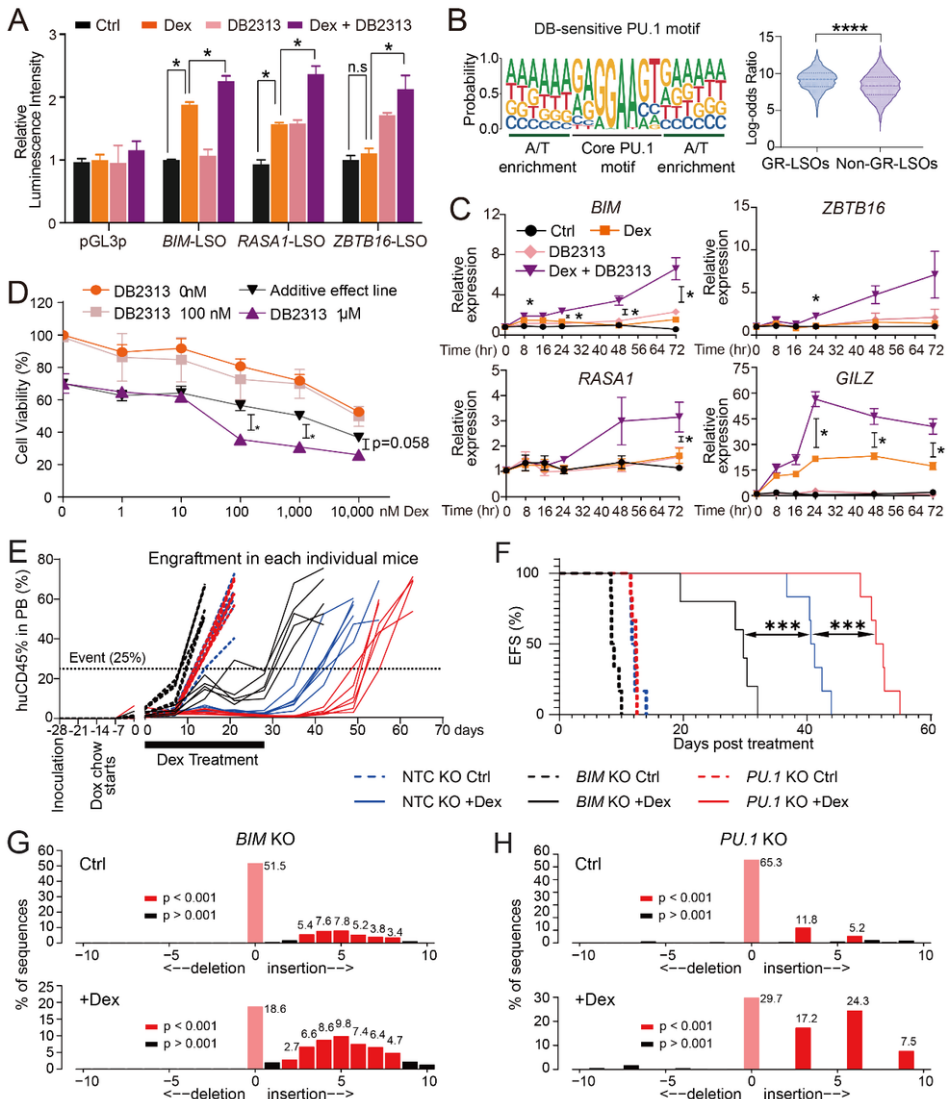
## Figure 6



### Figure 6

**PU.1 Knockdown and Combination Treatment with the PU.1 Inhibitor DB2313 in ALL-54S.**

(A) Luciferase reporter assay to determine the effect of a PU.1 inhibitor DB2313 on regulating *BIM* LSO, *RASA1* LSO and *ZBTB16* LSO in Nalm6 cells following dexamethasone treatment *in vitro*. DNA sequences of individual LSOs were cloned into 1 kb downstream of a luciferase cDNA in a pGL3P luciferase reporter vector. Renilla luciferase served as an internal control. The fold inductions were calculated by normalization to pGL3-promoter control. Data represent the mean ± SEM of three biological replicates. *, $p < 0.05$.

(B) Log-odds ratio for enrichments of the DB-sensitive PU.1 motif in GR-LSOs v.s. non-GR-LSOs. Left panel shows the motif of PU.1-binding lost sites induced by DB compound treatment as identified in (Taylor et al., under review[46]). Right panel displays log-odds ratios of motif enrichments in each dataset. DB, DB compounds of PU.1 inhibitors.

(C) Time course study of *BIM*, *ZBTB16*, *RASA1* and *GILZ* expression in Nalm6 exposed to dexamethasone (1 μM) alone or a combination treatment of 1 μM DB2313 and 1 μM dexamethasone. *GILZ*, which is a direct target of GR, was used as a positive control. Data represent the mean ± SEM of three biological replicates. *, $p < 0.05$.

(D) Cytotoxicity assay to determine synergistic effects of dexamethasone and DB2313 in inducing cell death of Nalm6. Data represent the mean ± SEM of three biological replicates. *, $p < 0.05$.

(E) Engraftment of ALL PDX cells with *BIM* KO, *PU.1* KO or Non-Transduced Control (NTC) cells in the peripheral blood (PB) of immune-deficient mice following dexamethasone treatment *in vivo*. The KO was induced by doxycycline feeding. Event is defined as 25% human cells in mouse PB. Dox, doxycycline. ***, p < 0.001.

(F) Event-free Survival (EFS) curves of mice engrafted with ALL PDXs of *BIM* KO, *PU.1* KO or NTC cells following saline/dexamethasone treatment *in vivo*.

(G-H) Indel profiles of *BIM* KO (G) and *PU.1* KO (H) ALL clones determined by Sanger sequencing following saline (Ctrl)/dexamethasone (Dex) treatment *in vivo*.

See also **Figure S5** and **S6**.

## Supplementary Files

This is a list of supplementary files associated with this preprint. Click to download.

- SupplementaryTableS1.xlsx
- SupplementaryTableS2.xlsx
- SupplementaryTableS3.xlsx
- SupplementaryTableS4.xlsx
- SupplementaryTableS5.xlsx
- SupplementaryTableS6.xlsx
- SupplementaryTableS7.xlsx
- SupplementaryTableS8.xlsx
- SupplementaryMaterials.docx